2

Solid State Research

1969

Prepared under Electronic Systems Division Contract AF 19(628)-5167 by

Lincoln Laboratory

MASSACHUSETTS INSTITUTE OF TECHNOLOGY

Lexington, Massachusetts

The work reported in this document was performed at Lincoln Laboratory, a center for research operated by Massachusetts Institute of Technology, with the support of the U.S. Air Force under Contract AF 19(628)-5167.

2

Solid State Research

1969

Issued 26 June 1969

Lincoln Laboratory

MASSACHUSETTS INSTITUTE OF TECHNOLOGY

Lexington, Massachusetts

ABSTRACT

This report covers in detail the solid state research work at Lincoln Laboratory for the period 1 February through 30 April 1969. The topics covered are Solid State Device Research, Materials Research, and Physics of Solids. The work formerly reported by the Optics and Infrared Group will henceforth appear in a separate report entitled "Optics Research" to be issued by the Optics Division.

Accepted for the Air Force
Franklin C. Hudson
Chief, Lincoln Laboratory Office

INTRODUCTION

I. SOLID STATE DEVICE RESEARCH

Spectral measurements in the frequency range from 10 to 130 cm^{-1} in magnetic fields from 0 to 30 kG of the far-infrared photoconductivity due to shallow donors in GaAs are reported. These measurements reveal peaks due to the isolated ($1s \rightarrow 2p$) and ($1s \rightarrow 3p$) transitions in addition to a broad continuum at higher energy. From the energy of these peak transitions and their splitting in a magnetic field, we obtain a donor ionization energy of 5.86 ± 0.02 meV and an effective mass of $0.0665 \pm 0.0005\ m_o$.

Electroluminescent metal-insulator-semiconductor (MIS) diodes have been fabricated using p-type ZnTe. The insulating layer was produced by bombarding the ZnTe with a dose of 5×10^{14} protons/cm^2 which at an energy of 400 keV produces a high-resistivity region approximately 5 μ deep. Broad red electroluminescence was observed in forward-bias breakdown with a quantum efficiency in excess of 2×10^{-3} at 77°K and 2×10^{-4} at 300°K.

Efficient doping of GaAs by ion implantation has been obtained using Se^+ ions. For a Se^+ dose of $3 \times 10^{12}/cm^2$ implanted at 400 keV, a peak carrier concentration of $2 \times 10^{17}/cm^3$ occurred at a depth of 750 Å, with a standard deviation of 500 Å. Integration of the excess carrier concentration caused by the implantation indicates that for this ion dose more than 50 percent of the implanted ions are electrically active. For larger doses, the doping efficiency decreases and the carrier concentration approaches a limiting value of approximately $10^{19}/cm^3$.

II. MATERIALS RESEARCH

X-ray diffraction measurements on metal- and tellurium-saturated $Pb_{1-x}Sn_xTe$ alloys have shown that deviations from stoichiometry have a marked effect on the lattice parameters of alloys containing more than about 50 mole percent SnTe. The results are consistent with published data which show that Vegard's law is obeyed over the whole composition range from PbTe to SnTe by alloy samples with sufficiently small deviations from stoichiometry.

The Hall coefficient and resistivity of undoped ZnSe single crystals have been measured at temperatures between 650° and 1000°C and at controlled zinc vapor pressures between 5 and 1000 torrs. The results show that at the temperatures and pressures investigated the electrical properties are determined by the concentration of a singly ionized native donor defect.

Photoluminescence due to tellurium substituted for sulfur or selenium has been observed at 4.2°K over the whole composition range of the ZnS-CdS and ZnS-ZnSe alloys. In both systems, the variation of the photoluminescence energy with composition is consistent with the isoelectronic trap model, according to which the trapping energy should become greater with increasing difference in electronegativity between the isoelectronic dopant and the host atom for which it substitutes.

Measurements of lattice parameter, density, electrical resistivity, Seebeck coefficient, and magnetic susceptibility have been made on a large number of single-phase samples of cubic TiO_x and VO_x with compositions spanning the extremely wide homogeneity range of each compound. Resistivity data for VO_x between 77° and 300°K fail to confirm the metal-semiconductor transition at about 120°K reported in the literature, but indicate that sufficiently oxygen-rich samples are probably semiconductors over the entire temperature range studied.

The compounds $Sr_4Ir_3O_{10}$ and $Sr_3Ir_2O_7$ have been synthesized at high pressures by reacting the appropriate amounts of Sr_2IrO_4 and IrO_2 at 1000°C. These compounds are the intermediate members in the series of compounds with the general formula $Sr_{1+x}IrO_{3+x}$ ($x = 0, \frac{1}{3}, \frac{1}{2}, 1$) whose structures consist of a number of perovskite units (ABX_3) interleaved with rock-salt layers (AX).

III. PHYSICS OF SOLIDS

Study of the band structure of the magnetic semiconductor EuO has continued. Splittings in the reflectivity spectrum on cooling to below the Curie point have been observed and interpreted as direct evidence for a spin-split conduction band.

An investigation of the magnetic interactions in the ferromagnetic conducting alloys $CoS_{2-x}Se_4$ has been initiated. Preliminary measurements in the magnetic transition region for $x = 0.1$ and 0.2 have raised some question regarding the order of the phase transition; it is hoped that differential thermal analysis may resolve this point. Concurrent with this experimental work, a theoretical study was carried out of the spin configuration which minimizes the classical Heisenberg exchange energy in the fcc lattice with first- and second-neighbor interactions. Our results are in contradiction to the spin configurations of CoSSe and $CoSe_2$ proposed by Adachi, et al., from neutron diffraction. If the latter configurations are correct, then there must be significant contributions to the energy from other than Heisenberg interactions.

Investigation of the local stability of the conical spiral spin configuration in normal cubic spinels shows that the spiral which gives good agreement with experiment for $CoCr_2O_4$ is actually unstable for the estimated values of the nearest-neighbor A-A, A-B, and B-B, and more-distant-neighbor B-B exchange interactions. The results demonstrate the existence of a new, previously unimagined configuration having nonzero Fourier components associated with more than one member of the $\vec{k} = (h,h,0)$ family — a configuration which appears to be more complicated than an epicone spiral.

Space-time symmetry restrictions on the thermogalvanomagnetic coefficients occurring for the magnetic field $H \neq 0$ have been examined further. Several previous tables have been supplemented.

The high-resolution thermal Brillouin scattering technique has been used to study the temperature dependence of the hypersonic (3- to 5-GHz) velocity and attenuation in liquid nitrogen along the saturated vapor line from the triple point to the normal boiling point. Since both the

velocity and attenuation results agree with previous measurements at megahertz frequencies, the acoustical dispersion due to the 2-GHz internal molecular vibration frequency is completely negligible.

Light emission has been observed from optically excited gold, copper, and gold-copper alloys. This emission, which involves states near the Fermi level, is consistent with optical absorption data.

Further work on light scattering by single-particle excitations in GaAs indicates that, although most of the anomalously large cross sections can be explained by spin-density fluctuations, the large temperature-dependent cross section observed in high-density samples (with incident and scattered polarization vectors parallel) requires a different mechanism. A study of resonant enhancement effects indicates that, despite the very small fluctuations in total charge density, fluctuations in the occupancy of electronic states can account for the parallel polarization cross section.

The theory of thermal self-trapping by CW laser beams in solids has been applied to a calculation of the half-power diameter in four different materials. Where experimental results exist (in two types of glass), the theory agrees reasonably well.

CONTENTS

ORGANIZATION

SOLID STATE DIVISION

P. E. Tannenwald, *Acting Head*
M. J. Hudson, *Assistant*
E. P. Warekois
C. R. Grant

SOLID STATE THEORY

H. J. Zeiger, *Leader*
M. M. Litvak, *Assistant Leader*

Brine, N. S.
Chiun, S. R.*
Dresselhaus, G. F.
Hamilton, D. C.
Hanus, J. G. C.
Kaplan, T. A.
Kleiner, W. H.
Landon, S. N.
Larsen, D. M.
Palm, B. J.†
Sigel, J. L.
Wilson, A. R. M.

SOLID STATE PHYSICS

J. G. Mavroides, *Leader*
G. B. Wright, *Assistant Leader*

Allen, J. W.
Barch, W. E.
Blum, F. A., Jr.
Brandt, R. C.
Burke, J. W.
Crooker, P. P.
DeFeo, W. E.
Dresselhaus, M. S.†
Dwight, K., Jr.
Feinleib, J.
Feldman, B.
Fulton, M. J.
Groves, S. H.
Henrich, V. E.
Johnson, E. J.
Kernan, W. C.
Kolesar, D. F.
Krag, W. E.
Melngailis, J.
Menyuk, N.
Nill, K. W.
Parker, C. D.
Pine, A. S.
Scouler, W. J.
Tichovolsky, E. J.*
Waldman, J.*
Weber, R.

ELECTRONIC MATERIALS

J. B. Goodenough, *Leader*
A. J. Strauss, *Associate Leader*

Anderson, C. H., Jr.
Arnott, R. J.
Banus, M. D.
Batson, D. A.
Brebrick, R. F., Jr.
Button, M. J.
Capes, R. N., Jr.
Delaney, E. J.
England, R. E.
Fahey, R. E.
Finn, M. C.
Hilton, T. W.
Iseler, G. W.
Kafalas, J. A.
Kasper, H. M.
LaFleur, W. J.
Lavine, M. C.†
Longo, J. M.
Mastromattei, E. L.
O'Connor, J. R.
Owens, E. B.
Plonko, M. C.
Raccah, P. M.
Reed, T. B.
Roddy, J. T.
Searles, I. H.
Smith, F. T. J.
Stack, T. E.
Steininger, J. M.
Temkin, R. J.*
Wheatley, G. E.

APPLIED PHYSICS

J. O. Dimmock, *Leader*
T. C. Harman, *Assistant Leader*
I. Melngailis, *Assistant Leader*

Brueck, S. R. J.*
Calawa, A. R.
Carter, F. B.
Cuswell, F. H.
Clough, T. F.
Donnelly, J. P.
Ferrante, G. A.
Foyt, A. G.
Krohn, L., Jr.
Lindley, W. T.
Mooradian, A.
Murphy, R. A.*
Oliver, M. R.*
Orphanos, W. G.
Paladino, A. E.
Phelan, R. J., Jr.
Stillman, G. E.
Ward, J. H. R., III
Wolfe, C. M.
Woods, R. J.
Youtz, P.

---

* Research Assistant

† Part Time

REPORTS BY AUTHORS ENGAGED IN SOLID STATE RESEARCH

15 February through 15 May 1969

PUBLISHED REPORTS

Journal Articles*

JA No.			
3082	Symmetry of the Ground Level of a Hamiltonian	W. H. Kleiner T. A. Kaplan	J. Math. Phys. 10, 236 (1969)
3275	Descriptions of Outer d Electrons in Thiospinels	J. B. Goodenough	J. Phys. Chem. Solids 30, 261 (1969)
3286	Homogeneity Ranges and Te_2-Pressure Along the Three-Phase Curves for Bi_2Te_3(c) and a 55-58 at. % Te, Peritectic Phase	R. F. Brebrick	J. Phys. Chem. Solids 30, 719 (1969)
3300	Metallic Inclusions and Cellular Substructure in $Pb_{1-x}Sn_xTe$ Single Crystals	J. F. Butler T. C. Harman	J. Electrochem. Soc. 116, 260 (1969)
3304	Self-Modulation, Self-Steepening, and Spectral Development of Light in Small-Scale Trapped Filaments	T. K. Gustafson† J-P. Taran† H. A. Haus† J. R. Lifsitz† P. L. Kelley	Phys. Rev. 177, 306 (1969)
3311	Effects of Pressure on the Magnetic Properties of MnAs	N. Menyuk J. A. Kafalas K. Dwight J. B. Goodenough	Phys. Rev. 177, 942 (1969)
3312	Effect of the Molecular Interaction Between Anisotropic Molecules on the Optical Kerr Effect. Field-Induced Phase Transition	J. Hanus	Phys. Rev. 178, 420 (1969)
3317A	Fermi Surface and Optical Properties of Copper	G. F. Dresselhaus	Solid State Commun. 7, 419 (1969)
3326	Characterization of Phases in the 50-60 at. % Region of the Bi-Te System by X-Ray Powder Diffraction Patterns	R. F. Brebrick	J. Appl. Crystal. 1, 241 (1968)

* Reprints available.

† Author not at Lincoln Laboratory.

Reports

JA No.			
3335	Transport Equation for Interacting Fermions in Random Scattering Centers. I. A Quasiparticle Description in the Macroscopic and Low Temperature Limit	J. L. Sigel P. N. Argyres	Phys. Rev. 178, 1016 (1969)
3336	Epitaxially Grown Guard Rings for GaAs Diodes	C. M. Wolfe W. T. Lindley	J. Electrochem. Soc. 116, 276 (1969)
3345	Optical Properties of Mg_2Si, Mg_2Ge and Mg_2Sn from 0.6 to 11.0 eV at 77°K	W. J. Scouler	Phys. Rev. 178, 1353 (1969)
3348	Temperature Dependence of Raman Linewidth and Shift in α-Quartz	A. S. Pine P. E. Tannenwald	Phys. Rev. 178, 1424 (1969)
3350	The P-T Phase Diagram of InSb at High Temperatures and Pressures	M. D. Banus M. C. Lavine	J. Appl. Phys. 40, 409 (1969)
3365	Photoluminescence of Metals	A. Mooradian	Phys. Rev. Letters 22, 185 (1969)
3371	Bismuth Doped $Pb_{1-x}Sn_xTe$ Diode Lasers with Low Thresholds	J. F. Butler T. C. Harman	IEEE J. Quant. Electron. QE-5, 50 (1969)
3386	Transient and Steady State Thermal Self-Focusing	R. L. Carman* A. Mooradian P. L. Kelley A. Tufts	Appl. Phys. Letters 14, 136 (1969)
3387	Infrared Transmission, Magnetic Birefringence, and Faraday Rotation in EuO	J. O. Dimmock C. E. Hurwitz T. B. Reed	Appl. Phys. Letters 14, 49 (1969)
3411	Report on International Conference on Silicon Carbide	J. R. O'Connor	J. Cryst. Growth 5, 152 (1969)
3421	Nuclear Linewidth Measurements of Mn^{55} in Antiferromagnetic $CsMnF_3$ and $RbMnF_3$	R. Weber M. H. Seavey*	Solid State Commun. 7, 619 (1969)
3426	GaAs Schottky Barrier Avalanche Photodiodes	W. T. Lindley R. J. Phelan, Jr. C. M. Wolfe A. G. Foyt	Appl. Phys. Letters 14, 197 (1969)
3436	$Pb_2M_2O_{7-x}$ (M = Re, Ir, Re) – Preparation and Properties of Oxygen Deficient Pyrochlores	J. M. Longo P. M. Raccah J. B. Goodenough	Materials Res. Bull. 4, 191 (1969)
3445	Experimental Techniques in Raman Spectroscopy	A. Mooradian	SPEX Speaker Ramalogs 2 (1969)

* Author not at Lincoln Laboratory.

MS No.			
2039	Critical Phenomena in Heisenberg Models of Magnetism	H. E. Stanley	Chapter 14, Solid State Physics, Nuclear Physics and Particle Physics, I. Saavedra, Ed. (W. A. Benjamin, Inc., New York, 1968); Proc. 9th Latin American School of Physics
2228	Interpolation Methods for Phonon Spectra in Crystals	G. F. Dresselhaus M. S. Dresselhaus	Intl. J. Quant. Chem. IIS, 333 (1968)
2307	Diffusion and Convection in Vapor Crystal Growth	T. B. Reed W. J. LaFleur A. J. Strauss	J. Cryst. Growth 3, 115 (1968)
2336	Light Scattering from Plasmons in Semiconductors	A. L. McWhorter	Proc. International Advanced Summer Physics Institute (Plenum, New York, 1969)

* * * * *

UNPUBLISHED REPORTS

Journal Articles

JA No.			
3173A	Statistical Thermodynamics of Nonstoichiometry in Non-Metallic Binary Compounds	R. F. Brebrick	Accepted by J. Solid State Chem.
3281	Crystallographic and Magnetic Properties of Perovskite and Perovskite-Related Compounds	J. B. Goodenough J. M. Longo	Accepted as a chapter in Landolt-Bornstein Tabellen (Springer-Verlag, Berlin)
3369	Inversion Asymmetry and Warping Induced Interband Magneto-Optical Transition in InSb	C. R. Pidgeon* S. H. Groves	Accepted by Phys. Rev.
3400	Magnetoreflection Studies in Arsenic	M. Maltz M. S. Dresselhaus	Accepted by Phys. Rev.
3412A	Experimental Comparison of Hartree-Fock and Slater Exchange Potentials in Aluminum from the Charge Density Point of View	P. M. Raccah V. E. Henrich	Accepted by J. Quant. Chem.
3417	Space-Time Symmetry Restrictions on Transport Coefficients. III. Thermogalvanomagnetic Coefficients	W. H. Kleiner	Accepted by Phys. Rev.
3423	Brillouin Scattering Study of Acoustic Attenuation in Fused Quartz	A. S. Pine	Accepted by Phys. Rev.

* Author not at Lincoln Laboratory.

Reports

JA No.			
3437	The Effect of Pressure and B-Cation Size on the Crystal Structure of $CsBF_3$ Compounds (B = Mn, Fe, Co, Ni, Zn, Mg)	J.M. Longo J.A. Kafalas	Accepted by J. Solid State Chem.
3441A	Magnetoreflection Studies on the Band Structure of Bismuth-Antimony Alloys	E.J. Tichovolsky J.G. Mavroides	Accepted by Solid State Commun.
3442	Effects of Light on the Charge State of InSb-MOS Devices	W.E. Krag R.J. Phelan, Jr. J.O. Dimmock	Accepted by J. Appl. Phys.
3447	Polymorphism in Selenospinels – A High Pressure Phase of $CdCr_2Se_4$	M.D. Banus M.C. Lavine	Accepted by J. Solid State Chem.
3449	Magnetoemission Experiments in $Pb_{1-x}Sn_xTe$	J.F. Butler	Accepted by Solid State Commun.
3460	Metallic Oxides	J.B. Goodenough	Accepted as a chapter in Progress in Solid State Chemistry (Pergamon Press, New York)
3463	Temperature and Compositional Dependence of Laser Emission in $Pb_{1-x}Sn_xSe$	T.C. Harman A.R. Calawa I. Melngailis J.O. Dimmock	Accepted by Appl. Phys. Letters
3468	Magnetospectroscopy of Shallow Donors in GaAs	G.E. Stillman C.M. Wolfe J.O. Dimmock	Accepted by Solid State Commun.

Meeting Speeches*

MS No.			
1954E	Conceptual Phase Diagram for Outer d Electrons in Solids	J.B. Goodenough	Societe Chimique de France, Paris, 14 March 1969
2338A	Meaning of an Anomaly in the X-Ray Scattering of ZnSe	P.M. Raccah	Seminar, Boston College, 19 March 1969
2378A	Exact Solution for a Linear Chain of Isotropically Interacting Classical Spins of Arbitrary Dimensionality	H.E. Stanley	American Physical Society, Philadelphia, Pennsylvania, 24-27 March 1969
2471	Spin-Space Group Analysis of $^4A_2 \rightarrow {}^2E$ Excitons in Cr_2O_3	J.W. Allen	
2472	Photoluminescence Due to Isoelectronic Te Traps in $Zn_{1-x}Cd_xS$ and $ZnS_{1-y}Se_y$ Alloys	G.W. Iseler A.J. Strauss	

* Titles of Meeting Speeches are listed for information only. No copies are available for distribution.

MS No.			
2473	Magneto-Optical Investigation of Bi-Sb Alloys	E. J. Tichovolsky J. G. Mavroides	American Physical Society, Philadelphia, Pennsylvania, 24-27 March 1969
2475	Inelastic Light Scattering from Semiconductor Magnetoplasmas	F. A. Blum	
2476	Polaron Zeeman Effect in AgBr	R. C. Brandt P. P. Crooker D. M. Larsen G. B. Wright	
2477	Temperature Dependence of Laser Emission in $Pb_{1-x}Sn_xSe$ Diodes in the Range $0 \leq x \leq 0.3$	A. R. Calawa I. Melngailis T. C. Harman	
2480	High Temperature Conductivity and Hall Coefficient of Zinc Telluride	F. T. J. Smith	
2482	Shubnikov-de Haas Measurements in $Pb_{1-x}Sn_xTe$	I. Melngailis T. C. Harman J. G. Mavroides J. O. Dimmock	
2483	Linear Wavevector Shifts in the Raman Spectrum of α-Quartz	A. S. Pine G. F. Dresselhaus	
2484	Effect of Deviations from Stoichiometry on Lattice Parameters of $Pb_{1-x}Sn_xTe$ Alloys	A. J. Strauss	
2485	Magnetic Energy Level Structure and Perturbation Theory	M. S. Dresselhaus P. R. Schroeder*	
2486	Efficient Doping of GaAs by Se^+ Ion Implantation	A. G. Foyt J. P. Donnelly W. T. Lindley	
2487	Reflectance of EuO from 0.5 to 11.0 eV	W. J. Scouler J. Feinleib J. O. Dimmock T. B. Reed	
2488	Infrared Absorption in Gd-Doped EuO	C. E. Hurwitz M. R. Oliver J. O. Dimmock T. B. Reed	
2493	Ion Implanted GaAs Avalanche Photodiodes	W. T. Lindley J. P. Donnelly A. G. Foyt R. J. Phelan, Jr.	

*Author not at Lincoln Laboratory.

Reports

MS No.			
2420F	Light Scattering from Semiconductors	A. Mooradian	Seminar, Harvard University, 19 February 1969
2452	Free Energy of Formation of Binary Compounds – An Atlas of Charts for High Temperature Chemical Calculations	T. B. Reed	American Chemical Society, Minneapolis, Minnesota, 17 April 1969
2465	Liquidus Surface in the Zn-Cd-Te Ternary System	J. M. Steininger A. J. Strauss	Electrochemical Society, New York, 9 May 1969
2466	The Role of Oxygen Pressure in the Control and Measurement of Composition in 3d Metal Oxides	T. B. Reed	Second Solid State Chemistry Conference, Scottsdale, Arizona, 21-25 April 1969
2506	Structural, Electrical and Magnetic Properties of Vacancy-Stabilized Cubic TiO and VO	M. D. Banus T. B. Reed	
2515	Evidence for a Continuous Sequence of Phases in the Bi-Te System	R. F. Brebrick	
2476A	Polaron Effects in Silver Bromide	R. C. Brandt	Seminar, University of Illinois, 9 May 1969
2499	The Effect of Pressure and B-Cation Size on the Crystal Structure of $CsBF_3$ Compounds (B = Mn, Fe, Co, Ni, Zn, Mg)	J. A. Kafalas J. M. Longo	Symposium on Crystal Structure at High Pressure, Seattle, Washington, 24-28 March 1969
2509	X-Ray Diffraction Studies on Cd_3As_2 and Zn_3As_2 at High Pressure	M. D. Banus M. C. Lavine	
2499A	Effect of High Pressure and Ion Size on Structure and Properties of ABX_3 Compounds	J. M. Longo	Technical Lecture, Naval Weapons Center, China Lake, California, 31 March 1969
2506A	Structural, Electrical and Magnetic Properties of Vacancy-Stabilized Cubic TiO and VO	M. D. Banus T. B. Reed	Seminar, Battelle Northwest Laboratories, Richland, Washington, 28 March 1969
2513	Ion Implantation in GaAs	A. G. Foyt	Seminar, Bell Telephone Laboratories, Murray Hill, New Jersey, 24 April 1969
2527	Comparison of Experimental and Theoretical Charge Densities for Si, Ge, and ZnSe	P. M. Raccah R. N. Euwema* D. J. Stuckel* T. C. Collins*	American Physical Society, Washington, D.C., 28 April – 1 May 1969

* Author not at Lincoln Laboratory.

MS No.			
2528	Light Scattering in Semiconductors	A. Mooradian	German Physical Society, Munich, Germany, 19 March 1969
2538	Cyclotron Waves and Landau Parameters	A. R. M. Wilson	Seminar, Bell Telephone Laboratories, Murray Hill, New Jersey, 5 Fehruary 1969
2539	The Deformation Potential in Silicon	W. E. Krag	Seminar, Boston College, 12 March 1969
2540	Fermi Surface and Optical Properties of Metals	G. F. Dresselhaus	Seminar, University of Maryland, 6 March 1969
2541, 2541A, 2541B	Derivation of a Quasiparticle Transport Equation for an Impure Fermi Liquid at Low Temperatures	J. L. Sigel	Seminar, Brown University, 6 March 1969; Seminar, Northeastern University, 11 March 1969; Seminar, University of Maryland, 21 April 1969
2543	Optical Imaging and Storage with MOS Structures	R. J. Phelan, Jr.	New England Chapter, Thin Film Division, American Vacuum Society, M. I. T. Lincoln Laboratory, 5 March 1969
2554, 2554A	Spectroscopy and Structure of Some Inorganic Solids	H. M. Kasper	Seminar, University of Michigan, 9 April 1969; Seminar, Arizona State University, 10 April 1969
2570	Ion Implantation in Semiconductors	J. P. Donnelly	Seminar, Carnegie-Mellon University, Pittsburgh, Pennsylvania, 17 April 1969
2571	Ion Implantation in Compound Semiconductors	A. G. Foyt	Seminar, M. I. T., 18 April 1969
2587	Polaron Effects in Solids	D. M. Larsen	Seminar, M. I. T., 9 May 1969

I. SOLID STATE DEVICE RESEARCH

A. MAGNETOSPECTROSCOPY OF SHALLOW DONORS IN GaAs

We have previously shown[1] that extrinsic photoconductivity in high-purity n-type epitaxial GaAs can provide fast, sensitive far-infrared detectors in the spectral range from 195 to 337 μ In this section, we report measurements of the photoconductivity spectra in the frequency range from 10 to 130 cm^{-1} in magnetic fields up to 30 kG; these measurements indicate, among other things, that in high-purity material the peak of the photoconductive response is due to excitation of bound electrons from the ground state of a hydrogenic donor to the first excited state and not to photoionization of the donor level.

The high-purity GaAs sample used in the measurements reported here was an epitaxial layer 68 μ thick which was grown on a high-resistivity GaAs substrate using an $AsCl_3$-Ga-H_2 flow system. Pure Sn ohmic contacts were alloyed to the sample in a reducing atmosphere. Analysis of Hall-effect and resistivity measurements gave a donor concentration of $4.8 \times 10^{13} cm^{-3}$, a total acceptor concentration of $2.1 \times 10^{13} cm^{-3}$, and a thermal donor ionization energy of 5.52 meV. The electron mobility was 8100 cm^2/volt-sec at 300°K, 205,000 cm^2/volt-sec at 77°K, and had a maximum of 340,000 cm^2/volt-sec at 40°K. The spectral measurements were made using an interferometer with the sample mounted in a light pipe at the center of a superconducting solenoid which was immersed in liquid helium. The photoconductivity spectra were corrected for beam splitter and source response by using a Golay cell reference which was assumed to be flat.

The spectral response of the photoconductivity per unit incident power is shown in Figs. I-1(a-d) for a temperature of 1.46°K and for magnetic fields of 0, 7.5, 15.0, and 29.9 kG. The response at zero magnetic field, shown in Fig. I-1(a), is characterized by a sharp peak at 35.5 cm^{-1}, a smaller peak at 42.2 cm^{-1}, and a broad continuum at higher frequencies. Our results indicate that these first two peaks are due to transitions between the ground state and the first two excited states of a shallow donor level in GaAs. Of the possible mechanisms, it seems likely that the main process responsible for this photoconductivity in our case is photoexcitation of electrons to the excited states followed by thermal ionization into the conduction band, since decreasing the temperature from 4.2° to 1.46°K reduced the amplitudes of the peaks relative to that of the broad continuum, while decreasing the electric field over two orders of magnitude caused essentially no change.

Assuming that the 35.5-cm^{-1} peak corresponds to the (1s → 2p) transition, a simple hydrogenic model for the donor levels predicts that the (1s → 3p) transition should occur at 42.1 cm^{-1}, in good agreement with the energy of the second peak, and that the donor ionization energy should be 47.3 cm^{-1} or 5.86 meV. This latter figure should be compared with a thermal ionization energy of 5.52 meV obtained from the Hall-effect analysis. Although the optical and thermal values are quite close, the difference is much larger than the experimental error in the two determinations. The significance of this difference will be discussed in a later publication.

The effect of a magnetic field on the photoconductivity spectra is shown in Figs. I-1(b) through (d) for fields of 7.5, 15.0, and 29.9 kG, respectively. Since the radiation which reaches

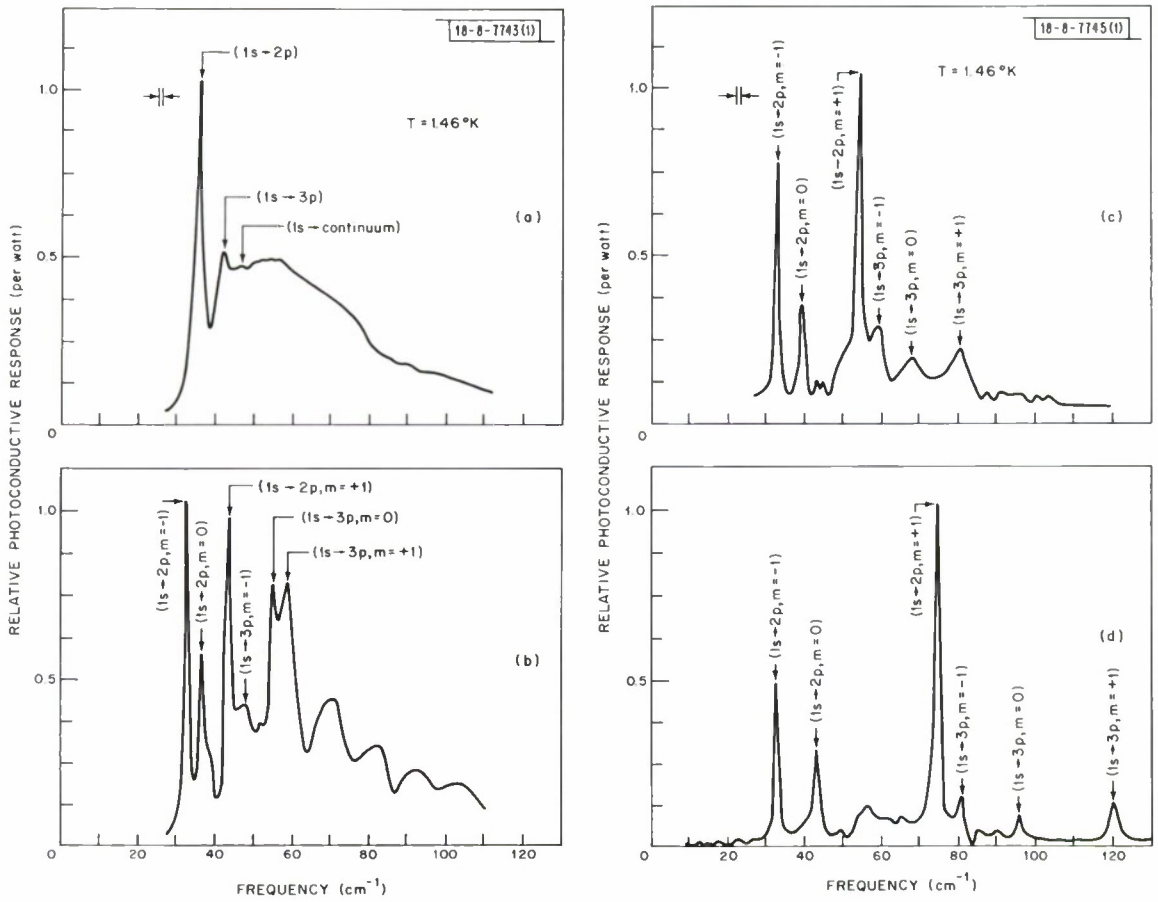

Fig. I-1. Spectral response of extrinsic photoconductivity of high-purity GaAs at 1.46°K at (a) H = 0 kG, (b) H = 7.5 kG, (c) H = 15.0 kG, and (d) H = 29.9 kG.

the detcctor after multiple reflections down the light pipe is completely depolarized, all 1s to higher p-state transitions are allowed and should be observed in the photoconductivity spectra. In particular, we have observed and identified photoconductivity peaks corresponding to the transitions to the (2p, $m_\ell = \pm 1$) and (3p, $m_\ell = \pm 1$) states, which split linearly in a magnetic field, as well as the transitions to the (2p, $m_\ell = 0$) and (3p, $m_\ell = 0$) states. Although the origin of the structure visible in the spectrum at 7.5 kG for frequencies greater than 60 cm^{-1} has not been determined definitely, it is probably due to transitions from the ground state to the higher excited impurity states. As the magnetic field is increased, the strength of the (1s → 2p) transitions increases in amplitudc relative to that of the other transitions including the continuum, and at the highest fields used (30 kG) the (1s → 2p, $m_\ell = +1$) transition becomes dominant. Although the fields uscd here are far from the high-field limit, it is interesting to note that the theory of Hasegawa and Howard[2] predicts that in the limit H → ∞, the (1s → 2p, $m_\ell = +1$) transition is the only one which survives. The experimental energies of the (1s → 2p) and (1s → 3p) transitions as a function of magnetic field are shown in Fig. I-2. The observed splittings of the (1s → 2p, $m_\ell = \pm 1$) and (1s → 3p, $m_\ell = \pm 1$) transitions are equal and are linear in H. This is the normal

Zeeman splitting, and for a simple hydrogenic donor is given by $\Delta E = e\hbar H/m^* c$, where m^* is the effective mass at the bottom of the conduction band. From the observed splitting, we calculate an effective mass of $m^* = 0.0665 \pm 0.0005\, m_o$. This compares well with the value of $m^* = 0.066 \pm 0.002\, m_o$ obtained from Faraday rotation measurements.[3]

As an internal self-consistency check, we can use our value of the effective mass and the measured static dielectric constant for GaAs to calculate the donor binding energy assuming a simple hydrogenic model. By using a dielectric constant[4] of 12.5, this calculation yields a donor binding energy of 5.79 meV, in reasonable agreement with the value of 5.86 meV obtained from the observed energies of the (1s → 2p) and (1s → 3p) transitions. The difference between these values is probably due to uncertainties in the value of the static dielectric constant.

The energy of the ground state (1s) and the two excited states (2p, $m_\ell = \pm 1$) of a hydrogenic impurity in an arbitrarily large magnetic field have been calculated by Larsen using a variational approach.[5] In Fig. I-3, we show a comparison between the experimental results for the (1s → 2p, $m_\ell = \pm 1$) transitions and the results of Larsen's theoretical calculation applied to GaAs. The fit was obtained using the above value of the effective mass obtained from the splitting and the observed zero-field position of the transition. The agreement is excellent and not only supports the variational calculation but also the simple hydrogenic model for these donor states.

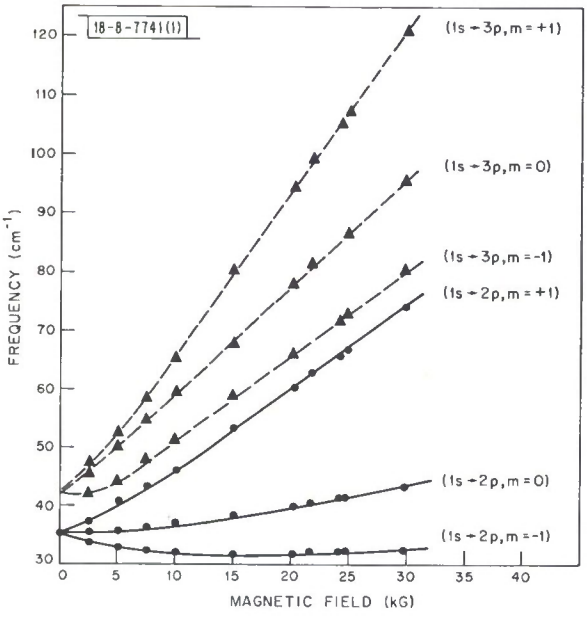

Fig. I-2. Energies of (1s → 2p) and (1s → 3p) transitions as a function of magnetic field.

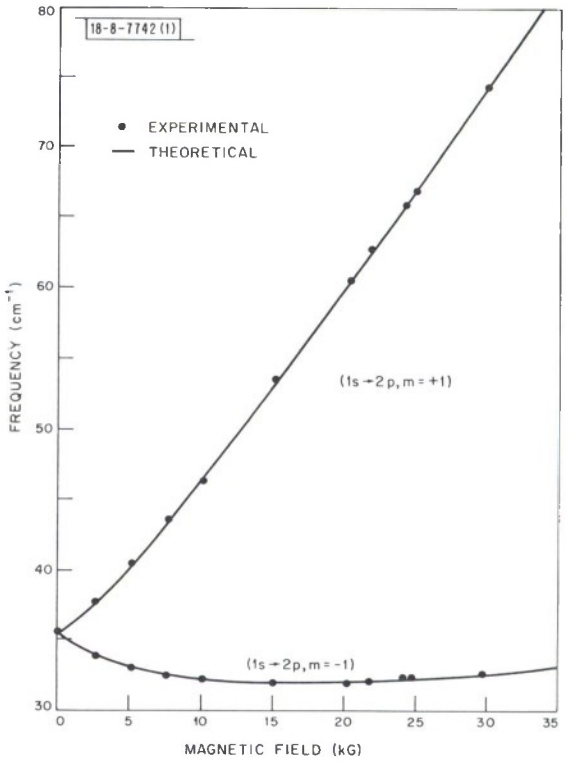

Fig. I-3. Experimental and theoretical magnetic field dependence of (1s → 2p, $m_\ell = \pm 1$) transition energies. Data points are experimental points for corresponding transition, and solid curves are from Larsen's calculation (Ref. 5).

We can conclude that this model provides a remarkably accurate description of the shallow donor states in GaAs. This accuracy has allowed us to obtain very precise values of the optical donor ionization energy and electron effective mass in addition to an identification of the absorption process responsible for the far-infrared photoconductivity observed in high-purity GaAs.

G. E. Stillman
C. M. Wolfe
J. O. Dimmock

B. MIS ELECTROLUMINESCENT DIODES IN ZnTe

We previously reported[6] that proton radiation can be used to create high-resistivity layers in p-ZnTe. Recently, we have used this technique to fabricate MIS (metal-insulator-semiconductor) electroluminescent diodes.

The p-ZnTe samples used in these experiments were annealed Bridgman-grown crystals with a carrier concentration of $2 \times 10^{16}/cm^3$ and a mobility of $80\,cm^2/volt\text{-}sec$. Each sample was bombarded with 5×10^{14} protons/cm^2 of a selected fixed energy which ranged from 50 to 400 keV. Electrical measurements indicated that the resistivity of the bombarded layers was greater than 10^9 ohm-cm. The width of the high-resistivity layer was linear with proton energy and was approximately 1.2 μ for 100-keV protons.

MIS diodes which exhibited sharp avalanche breakdown in both bias directions were fabricated by this technique using plated gold as the metallic layer. Forward breakdown voltages (p-type substrate positive) ranged from 6 volts for 50-keV protons to 80 volts for 400-keV protons. Broad red electroluminescence was observed in forward-bias breakdown. We have obtained a quantum efficiency of 2×10^{-3} at 77°K and 2×10^{-4} at 300°K by measuring the light coming from the back of the diode using a calibrated S-1 photomultiplier. However, these quantum efficiencies must be considered as lower limits because some of the light is absorbed in passing through the bulk ZnTe, which is approximately 6 mils thick.

J. P. Donnelly
A. G. Foyt
W. T. Lindley

C. EFFICIENT DOPING OF GaAs BY Se^+ ION IMPLANTATION

Efficient doping of GaAs using Se^+ ions implanted at 400 keV was previously reported.[7] In this section, we give a more detailed report on this work and include some additional results on the implanted sheet carrier concentration as a function of Se^+ ion dose for implantations carried out at both room temperature and 500°C. Although previous work on ion implantation into GaAs has shown that doping and type conversion can be achieved using Zn and Te ions,[8-11] we believe that this work is the first to demonstrate efficient doping in GaAs using this technique.

Both p- and n-type substrates were used in these experiments. The samples, approximately $10 \times 5 \times 1$ mm, were cut, lapped, and free-etched using standard techniques. They were then coated with 1500 Å of SiO_2 to prevent thermal etching during subsequent heat treatments. The samples were then placed in the Van de Graaff generator and implanted with Se^+ ion doses between 2×10^{12} and $2 \times 10^{15}/cm^2$. Although implantations were done with the samples at various temperatures between room temperature and 500°C, the most efficient doping occurred at the

highest temperature. Consequently, most of our experiments were done with the samples at 500°C during implantation. The samples were then removed from the holder and post-annealed at 800°C for 2 minutes.

Following implantation and annealing, the carrier concentration profile was measured in the n-type samples using the differential capacitance-voltage method.[12] To do this, 15-mil-square gold Schottky barrier contacts were plated onto the implanted layer using the SiO_2 as a plating mask and the capacitance of each of these diodes was then measured as a function of voltage. A typical result is shown in Fig. I-4 where we show the profile of a sample with a background carrier concentration of $2 \times 10^{16}/cm^3$ which was implanted with a 400-keV Se^+ dose of $3 \times 10^{12}/cm^2$. As may be seen, a peak concentration of $2 \times 10^{17}/cm^3$ was observed at a depth of approximately 750 Å. The concentration decreases from this peak with increasing depth, approaching the background carrier concentration. The observed standard deviation of 500 Å is approximately that expected from Lindhard range theory.[13] However, the peak carrier concentration is closer to the sample surface than expected from this model because of the 1500-Å SiO_2 layer.

We may obtain an estimate of the doping efficiency for the implanted ions by integrating the additional carrier concentration in the shaded region of Fig. I-4. This calculation showed that the number of additional carriers in this region is approximately 50 percent of the total number of the implanted ions. Since some of the implanted ions were stopped in the SiO_2 layer, and others were stopped in the region of the sample near the surface which could not be measured with this technique, we see that the doping efficiency of the implanted Se^+ ions is actually considerably greater than this estimate of 50 percent.

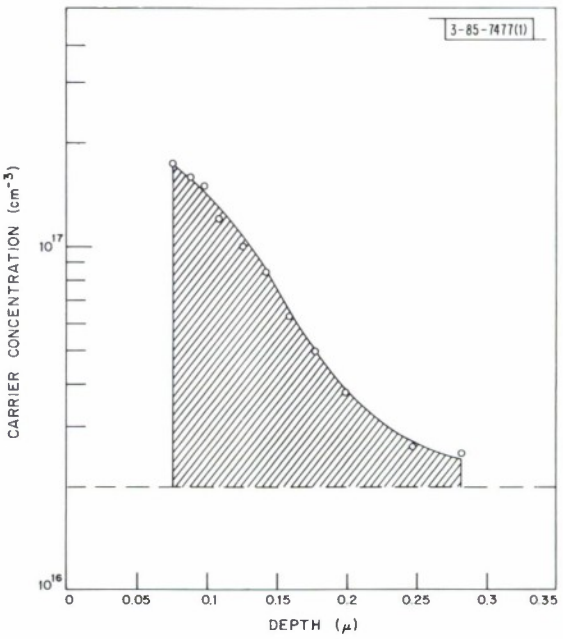

Fig. I-4. Carrier concentration profile for sample of n-GaAs ($n \sim 2 \times 10^{16}/cm^3$) which was implanted with 400-keV Se^+ ion dose of $3 \times 10^{12}/cm^2$. Additional carrier concentration in shaded region is approximately 50 percent of total ion dose.

We were not able to extend this technique of measurement to samples implanted with heavier doses of selenium because the range of depths covered between forward conduction and reverse-bias breakdown in the Schottky barrier diode was too small. We therefore turned to implantations into p-type samples, and used van der Pauw[14] – Hall-effect measurements on the implanted layer to explore the effects of larger doses.

These p-type samples were implanted and annealed in the same manner as the n-type samples. After being annealed, the implanted layer was contacted using plated and alloyed gold-tin contacts, with a gold-zinc contact used for the p-type substrate. Hot point probe measurements made on these contacts in the dark indicated that the implanted region had been converted to n-type, while the substrate remained p-type.

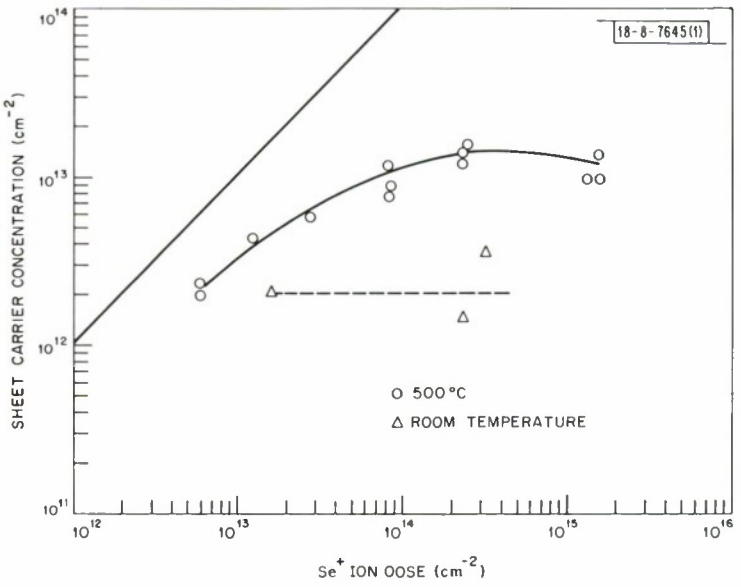

Fig. I-5. Measured sheet carrier concentration vs total ion dose for 400-keV Se^+ ions implanted into p-GaAs ($p \sim 3 \times 10^{16}/cm^3$). Straight line corresponds to 100-percent doping efficiency.

In order to reduce contact effects in the van der Pauw – Hall-effect measurements, a clover-leaf pattern was etched in the sample around four contacts on the implanted layer. Current-voltage measurements between these contacts showed that the four contacts on the implanted layer were ohmic, while good diode characteristics were observed between each of these contacts and the p-type substrate. The leakage current between the implanted layer and the substrate was sufficiently low to insure that the substrate could be neglected in these measurements. In Fig. I-5, the measured sheet carrier concentration is shown as a function of the number of implanted Se^+ ions; the straight line corresponds to a 100-percent doping efficiency. As may be seen, implantations done at room temperature exhibit a lower doping efficiency than those carried out at 500°C. For a sample implanted at 500°C with a dose of $6 \times 10^{12}/cm^2$ Se^+ ions, these van der Pauw – Hall measurements indicate that about 35 percent of the total number of ions implanted are electrically active. However, it should be noted that this measurement underestimates the doping efficiency and should be considered a lower limit because (1) some of the ions are stopped in the SiO_2, and (2) variations in carrier concentration and mobility with depth in the implanted layer lead to a measured sheet carrier concentration which is smaller than the actual value.[15,†] Stripping techniques have shown that for ions implanted into silicon, the measured sheet carrier concentration was between 50 and 80 percent of the actual value.[16]

For larger doses of selenium, the sheet carrier concentration approaches a limiting value of about $2 \times 10^{13}/cm^2$. If we assume that the Lindhard range theory remains valid for these larger doses, the peak carrier concentration at which we begin to observe the saturation is approximately $10^{19}/cm^3$. This limit corresponds to that observed for selenium incorporated into

† By using the Schwartz inequality, it can be shown that the van der Pauw measurement will always underestimate the carrier concentration if the mobility varies within the implanted layer.

the GaAs during crystal growth,[17] where a carrier concentration of $2 \times 10^{19}/cm^3$ is observed for a selenium concentration of $10^{21}/cm^3$. Typical mobility values for the implanted layers are 1500 to 2000 cm^2/volt-sec. For a dose of $2 \times 10^{14}/cm^2$, a sheet resistance of 250 ohms/square was observed.

We have also fabricated junction diodes using this technique. These diodes, fabricated on p-type substrates ($p \sim 5 \times 10^{16}/cm^3$) had junction diameters of about 5 mils. The diodes were separated and guard-ringed using the proton bombardment technique,[18] which converts both the p- and n-type GaAs around the diode into semi-insulating material. These diodes had sharp reverse breakdowns at 20 to 24 volts. In forward bias, the diodes emit bandgap radiation at currents of 1 mA, as observed through an infrared image converter with an S-1 photocathode. Capacitance measurements indicate that these junctions are abrupt. There is no indication of the presence of an intrinsic region as has been reported by Hunsperger, et al.,[19] for diodes fabricated by the implantation of 70-keV Zn^+ ions into n-type GaAs.

A. G. Foyt
J. P. Donnelly
W. T. Lindley

REFERENCES

1. G. E. Stillman, C. M. Wolfe, I. Melngailis, C. D. Parker, P. E. Tannenwald, and J. O. Dimmock, Appl. Phys. Letters 13, 83 (1968), DDC 681589.
2. H. Hasegawa and R. E. Howard, J. Phys. Chem. Solids 21, 179 (1961).
3. H. Piller, J. Phys. Soc. Japan 21S, 206 (1966).
4. C. Hilsum and A. C. Rose-Innes, Semiconducting III-V Compounds (Pergamon Press, New York, 1961), p. 181.
5. D. M. Larsen, J. Phys. Chem. Solids 29, 271 (1968).
6. Solid State Research Report, Lincoln Laboratory, M.I.T. (1968:3), p. 10, DDC 678534, H-899.
7. Solid State Research Report, Lincoln Laboratory, M.I.T. (1969:1), p. 3, DDC 687100.
8. J. W. Mayer, O. J. Marsh, R. Mankarious, and R. Bower, J. Appl. Phys. 38, 1975 (1967).
9. P. E. Roughan and K. E. Manchester, J. Electrochem. Soc. 116, 278 (1969).
10. R. G. Hunsperger and O. J. Marsh, J. Electrochem. Soc. 116, 488 (1969).
11. J. B. Schroeder and H. D. Dieselman, Proc. IEEE 55, 125 (1967).
12. C. O. Thomas, D. Kahng, and R. C. Manz, J. Electrochem. Soc. 109, 1055 (1962).
13. J. Lindhard, M. Scharff, and H. Schiott, Kgl. Danske Videnskab, Selskab, Mat. Fys. Medd. Dan. Vid. Selsk. 33, 1 (1963).
14. L. J. van der Pauw, Phillips Res. Repts. 13, 1 (1958).
15. P. L. Petritz, Phys. Rev. 110, 1254 (1958).
16. J. W. Mayer, O. J. Marsh, G. A. Shifrin, and R. Baron, Can. J. Phys. 45, 4073 (1967).
17. R. W. Fane and A. J. Goss, Solid State Electron. 6, 383 (1963).
18. A. G. Foyt, W. T. Lindley, C. M. Wolfe, and J. P. Donnelly, Solid State Electron. (to be published).
19. R. G. Hunsperger, O. J. Marsh, and C. A. Mead, Appl. Phys. Letters 13, 295 (1968).

II. MATERIALS RESEARCH

A. EFFECT OF DEVIATIONS FROM STOICHIOMETRY ON LATTICE PARAMETERS OF $Pb_{1-x}Sn_xTe$ ALLOYS

The compounds PbTe and SnTe form a complete series of solid solutions with rock-salt structure. For PbTe, the entire homogeneity range is so narrow that deviations from stoichiometry do not cause any detectable variation in lattice parameter, but for SnTe the change in composition across the homogeneity range is sufficient to produce an appreciable variation. We have made x-ray diffraction measurements on metal- and Te-saturated $Pb_{1-x}Sn_xTe$ alloys which show that deviations from stoichiometry also have a marked effect on the lattice parameters of alloys containing more than about 50 mole percent SnTe.

Samples were prepared from weighed quantities of the semiconductor grade elements. The ratio of metal (Pb + Sn) atoms to Te atoms was 53 to 47 for metal-saturated samples and 47 to 53 for Te-saturated samples. These proportions were chosen in order to be sure that at equilibrium each sample would be a two-phase mixture consisting of the saturated alloy and a small quantity of either excess metal or excess Te. The elements were melted together at about 950°C and quenched to form ingots, which were then crushed to a particle size of about 1 mm, homogenized by annealing at 750°C for 7 days, ground to pass a 325-mesh sieve, and finally annealed at 350°C for at least 4 days in order to remove work damage. X-ray diffraction patterns were obtained with a Debye-Scherrer camera, and lattice parameter (a_o) values were calculated to an accuracy of ±0.001 Å by a least-squares extrapolation method.

The experimental results are shown in Fig. II-1, where a_o is plotted against $(1 - y)$, the mole fraction of PbTe weighed out. The reason for distinguishing the nominal mole fraction $(1 - y)$

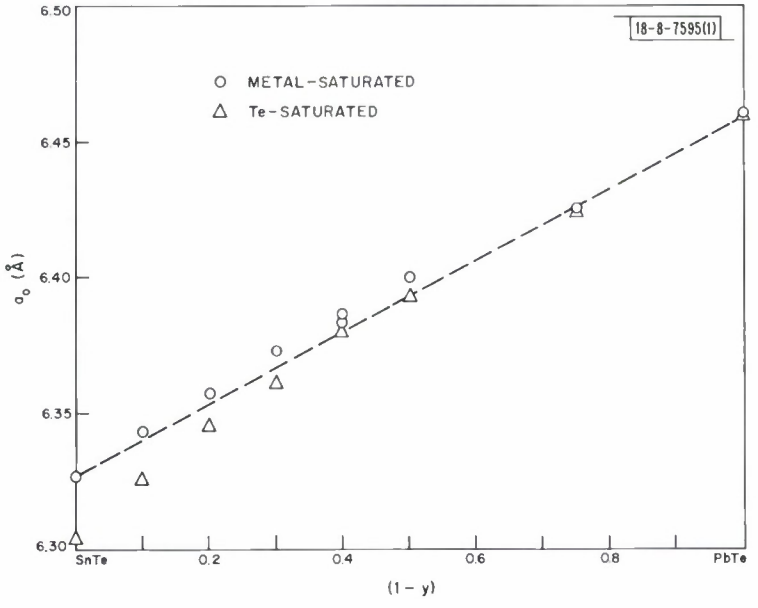

Fig. II-1. Lattice parameter of metal- and Te-saturated $Pb_{1-x}Sn_xTe$ alloys as a function of nominal mole fraction $(1 - y)$ of PbTe.

from the actual mole fraction $(1 - x)$ will be discussed below. Within the limit of experimental error, the a_o values for Pb- and Te-saturated PbTe agree with each other and with the literature values. Agreement between the two different samples is also obtained for $(1 - y) = 0.75$. For alloys with $(1 - y) = 0.5$ or less, however, a_o is appreciably higher for the metal-saturated sample than for the Te-saturated one, and the difference generally increases with increasing SnTe content. The largest difference, 0.023 Å, is observed for SnTe. The a_o values for Sn-saturated SnTe (6.327 Å) and Te-saturated SnTe (6.304 Å) are in good agreement with literature values. These results show that the width of the homogeneity range for $Pb_{1-x}Sn_xTe$ alloys increases with increasing SnTe content, becoming large enough at about 50 mole percent SnTe for deviations from stoichiometry to cause a significant variation in a_o.

By means of lattice parameter measurements on thin films with carrier concentrations below $10^{20}\,cm^{-3}$, Bis and Dixon[1] have shown that Vegard's law is obeyed by $Pb_{1-x}Sn_xTe$ alloys with sufficiently small deviations from stoichiometry. Since it has been found that metal-saturated PbTe and SnTe both have the same a_o values as would be observed for the stoichiometric compounds, the metal-saturated alloys should also have the same a_o values as the corresponding stoichiometric samples. Therefore, the metal-saturated alloys would be expected to obey Vegard's law. However, it is seen in Fig. II-1 that the a_o values for metal-saturated samples containing up to 50 mole percent PbTe are significantly higher than the Vegard's law values, which are given by the dashed straight line. These apparent deviations result because the mole fraction of PbTe incorporated in the alloy $(1 - x)$ is systematically higher than the nominal value $(1 - y)$.

Evidence for differences between $(1 - x)$ and $(1 - y)$ has been obtained by a series of experiments in which $(1 - y)$ was kept at 0.2 while the atom fraction of Te was varied between 0.47 and 0.53. The results are shown in Fig. II-2, where a_o is plotted against z, the atom fraction of Te weighed out. For metal-saturated alloys, it is seen that a_o increases linearly as z decreases

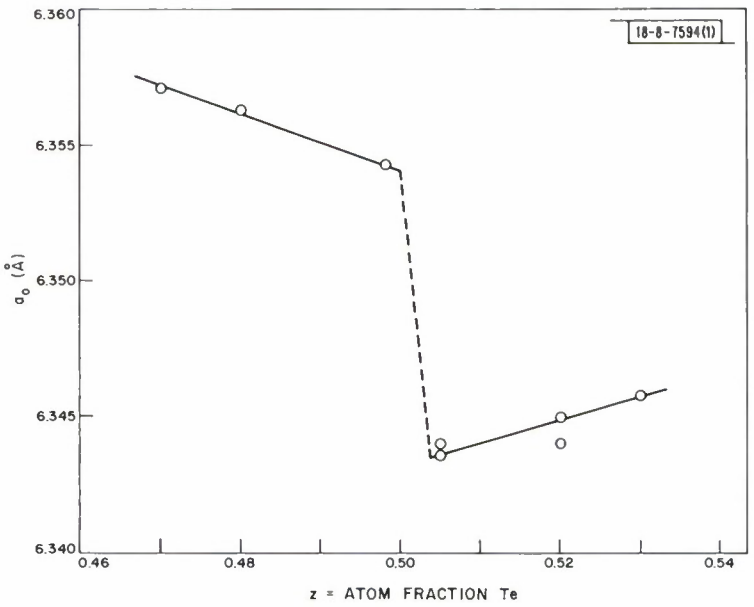

Fig. II-2. Lottice porometer of $Pb_{1-x}Sn_xTe$ allays present in samples with overall compositions of $(Pb_{0.2}Sn_{0.8})_{1-z}Te_z$.

from 0.495 to 0.47. If we assume that all these alloys are essentially stoichiometric, this increase in a_o confirms the increase in $(1 - x)$ as the overall metal-to-Te ratio is increased. The values of $(1 - x)$ and $(1 - y)$ should be equal for $z = 0.5$, since for that composition the sample will be essentially single phase. Therefore, extrapolation of the straight line to $z = 0.5$ should give the lattice parameter for $(1 - x) = (1 - y) = 0.2$. This extrapolation gives $a_o = 6.354$ Å, exactly the Vegard's law value. Thus, the present results are consistent with the Vegard's law behavior found by Bis and Dixon.[1]

The data for Te-rich compositions in Fig. II-2 show that $(1 - x)$ differs from $(1 - y)$ for these samples also. As in the metal-rich case, the value of $(1 - x)$ increases as the system departs further and further from the stoichiometric composition. For this reason, the difference between the values of a_o for the extreme values of z (0.47 and 0.53) is equal to the difference between the values of a_o found by extrapolating to the phase boundaries of the alloy with $(1 - x) = 0.2$. If it is assumed that this is also true for the other alloy compositions studied, the a_o differences shown in Fig. II-1 can be used to obtain estimates for the width of the homogeneity range for the alloys as a function of mole percent PbTe.

A. J. Strauss

B. EVIDENCE FOR A NATIVE DONOR IN ZnSe

Although native defects associated with deviations from stoichiometry are known to have an important influence on the electrical properties of several II-VI compounds,[2] their role in ZnSe has not been established. In order to investigate this role, we have measured the Hall coefficient and resistivity of undoped ZnSe single crystals at temperatures between 650° and 1000°C and at controlled zinc vapor pressures between 5 and 1000 torrs. The results show that at the temperatures and pressures investigated, the electrical properties are determined by the concentration of a singly ionized native donor, but that the high conductivities observed at room temperature for ZnSe samples annealed in liquid zinc are probably due to foreign donor impurities, rather than to the native defects.

The ZnSe crystals, all of which had the cubic zinc-blende structure, were grown from the vapor phase by two different methods. In the first method, hydrogen purified by a platinum-palladium alloy filter entered a fused quartz apparatus and was divided into two separate streams, which were passed over heated boats containing 99.999-percent pure zinc or selenium, respectively. The two streams containing the elements were then recombined in a growth region at about 1100°C, where crystals in the form of platelets about 5 to 10 mm in diameter and 1 to 2 mm thick were obtained. The other crystals were grown by a modification of the Piper-Polich[3] technique. In this second method, a fused quartz ampoule was pulled through a temperature gradient, causing sublimation of a charge of polycrystalline ZnSe located at the hotter end of the ampoule and deposition of a large-grained ZnSe boule at the colder end.

The apparatus used for electrical measurements is shown schematically in Fig. II-3. The desired vapor pressure of zinc vapor is established by adjusting the temperature of a reservoir of pure zinc located at the bottom of a fused quartz tube. The reservoir and sample temperatures are controlled independently. Two graphite conical seals are used to contain the high-temperature vapor. The total pressure in the apparatus is maintained at one atmosphere by using a continuous flow of high-purity argon controlled by means of a manostat and vacuum pump. Contact to the sample, which is in the form of a square plate, is made by four graphite knife edges. The contacts

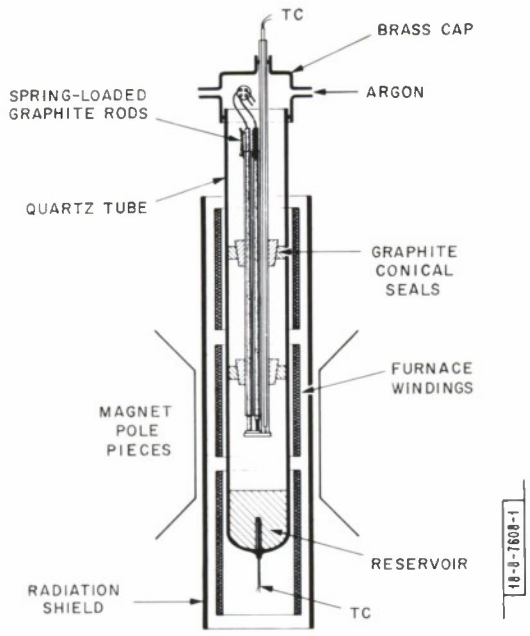

Fig. II-3. Schematic drowing of opporotus far Holl coefficient and resistivity meosurements at high temperatures and cantrolled vapor pressures.

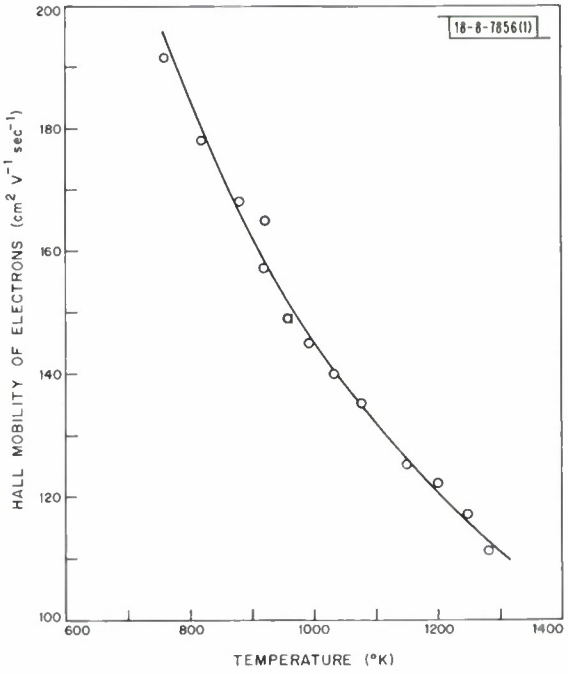

Fig. II-4. Holl mobility af electrons in ZnSe os o functian of temperature.

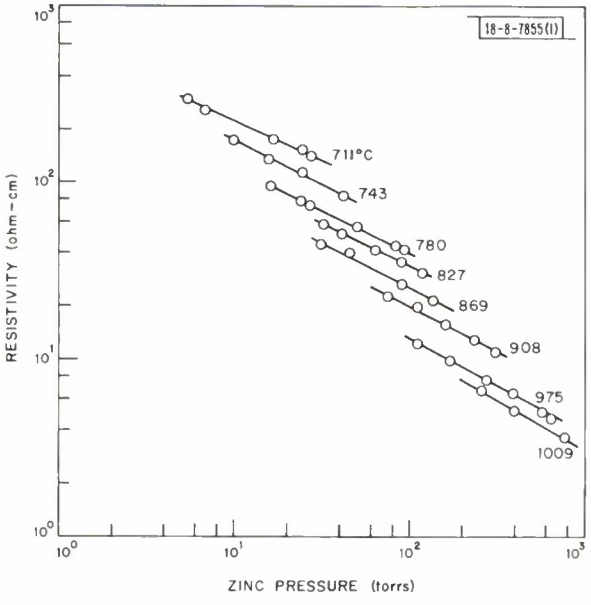

Fig. II-5. Resistivity af ZnSe at voriaus temperatures as o functian af zinc partial pressure p_{Zn}.

are ohmic above 650°C but become weakly rectifying at lower temperatures. The whole apparatus is placed inside a three-zone furnace insulated by means of a semitransparent gold radiation shield which is small enough in diameter to be placed between the pole pieces of a conventional 4-inch electromagnet. Both Hall and resistivity measurements are made by the DC van der Pauw method, with a magnetic field of 5.3 kOe and a total voltage drop across the sample of less than 1 volt.

The Hall coefficient measurements show that all the samples are n-type, as expected from the fact that p-type conductivity in ZnSe has been reported only for a few samples heavily doped with acceptor impurities. In Fig. II-4, the Hall mobility ($\mu = R_H/\rho$) for a typical crystal is plotted against temperature. Since the measured mobilities do not depend on carrier concentration or vary appreciably from sample to sample, the curve shown gives the lattice mobility of electrons in ZnSe. In the temperature range studied, the lattice mobility is probably limited by polar optical scattering,[4] but a detailed comparison with theory cannot be made because the temperature dependence of such quantities as the static dielectric constant is not known.

The resistivity of a typical specimen at a number of temperatures is plotted in Fig. II-5 as a function of zinc partial pressure p_{Zn}. At each temperature, the resistivity is proportional to $(p_{Zn})^{-m}$, and the carrier concentration therefore varies as $(p_{Zn})^{m}$, where $m = 0.5 \pm 0.05$. The measured resistivities are independent of the previous treatment of the specimen and are reproducible to ±10 percent between specimens. This reproducibility, particularly between crystals grown by two different techniques, as well as the fact that the resistivity depends on p_{Zn}, indicates that the carrier concentration is determined by the concentration of a native donor defect, rather than by impurities. Since the donor concentration increases with increasing zinc pressure and therefore with increasing zinc content, the defect is either a zinc interstitial or a selenium vacancy. The value of $m = 0.5$ indicates that the defect is singly ionized in the temperature region investigated.

In Fig. II-6, the variation of carrier concentration with reciprocal temperature at $p_{Zn} = 20$ torrs is shown by the lower line. The slope of such a plot is $\Delta H_f/2k$, where ΔH_f is the apparent

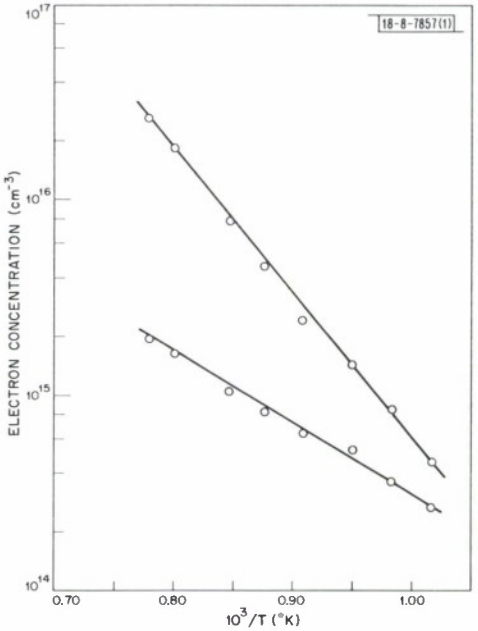

Fig. II-6. Carrier cancentratian in ZnSe as a functian af recipracal absolute temperature. Upper line: along zinc-rich salidus; lawer line: samples equilibrated at p_{Zn} = 20 tarrs.

enthalpy of formation of the singly ionized donor, and k is the Boltzmann constant. The slope in Fig. II-6 gives a value of 1.6 ± 0.2 eV for ΔH_f. Within the limit of error, the same value is obtained from similar plots for other values of p_{Zn}.

The data of Fig. II-5 can be used to obtain very good values for the carrier concentrations along the Zn-rich solidus of ZnSe. In this temperature region, p_{Zn} over the liquid phase in equilibrium with Zn-saturated ZnSe is almost the same as that over pure liquid Zn, since the solubility of ZnSe in liquid Zn is extremely low.[5] Therefore, the carrier concentrations at the Zn-rich solidus will agree to within a few percent with those obtained by extrapolating the resistivity isotherms of Fig. II-5 to the pressures over pure liquid Zn. Carrier concentrations obtained by this extrapolation are shown as a function of reciprocal temperature by the upper line in Fig. II-6. Since the carrier concentration is proportional to the concentration of Zn in excess of the stoichiometric composition, the slope of this line shows that the solubility of Zn in ZnSe is retrograde over the temperature range investigated.

It has been reported[6] that ZnSe samples with resistivities as low as 0.1 ohm-cm at room temperature have been prepared by annealing in liquid Zn at elevated temperatures. We obtained resistivities orders of magnitude higher when specimens were Zn-saturated at temperatures up to 1000°C and then quenched to room temperature, presumably because the amount of excess Zn dissolved in the lattice decreased greatly during cooling. Such a rapid reduction is consistent with the speed at which equilibrium was attained in our experiments at high temperatures. For example, the time required to reach the equilibrium resistivity after a change in zinc pressure decreased from approximately 100 minutes at 650°C to less than 15 minutes at 950°C. The carriers in the low-resistivity samples reported in the literature are apparently due to the ionization of donor impurities, which were compensated in the as-grown samples by acceptor impurities removed by the solvent extraction process[7] during annealing in liquid Zn.

F. T. J. Smith

C. PHOTOLUMINESCENCE DUE TO ISOELECTRONIC Te TRAPS IN $Zn_{1-x}Cd_xS$ AND $ZnS_{1-y}Se_y$ ALLOYS

Isoelectronic traps which are efficient radiative recombination centers have been identified in III-V and II-VI compounds. Thomas and co-workers[8,9] have investigated GaP doped with N or Bi, ZnTe doped with oxygen, and CdS doped with Te. We have previously reported the properties of oxygen in ZnTe-ZnSe and ZnTe-CdTe alloys.[10] The results obtained for these alloys are consistent with the Thomas model, according to which the trapping energy should increase with increasing difference in electronegativity between the isoelectronic dopant and the host atom for which it substitutes. We have now investigated the behavior of the Te photoluminescence spectrum over the whole composition range of the CdS-ZnS and ZnS-ZnSe alloys. The results for these systems are also consistent with the isoelectronic trap model.

The Te-doped alloys were prepared by annealing weighed mixtures of the powdered binary compounds in evacuated, sealed quartz ampoules. One set of CdS, ZnS, ZnSe, and ZnTe samples was purchased from Eagle Picher and another was prepared from the elements in our laboratory. The mixed powders were annealed at 1075°C for 2 to 3 days and quenched in water. Photoluminescence was excited by 3650-Å radiation from a high-pressure Xe-Hg lamp.

For CdS moderately doped with Te, two emission bands in the visible are observed in photoluminescence or cathodoluminescence[9] experiments at 4.2 °K. For very lightly Te-doped samples only the high-energy band (A) appears, while for heavily doped samples only the low-energy band (B) is seen. Both bands are probably phonon broadened, but no phonon structure has been observed. Cuthbert and Thomas[9] have suggested that band A corresponds to the decay of an exciton bound to a Te atom on an S-site, and that band B corresponds to the decay of an exciton bound to two Te atoms on nearest-neighbor S-sites. They found that at room temperature the fluorescence quantum efficiency for cathodoluminescence is about 30 percent for band B, and about 10 percent for band A.

Our photoluminescence data, obtained at 4.2 °K for Te-doped CdS-ZnS alloys, are summarized in Fig. II-7 where the photon energy at the peak of each band is plotted vs the mole fraction of ZnS. The energy gap for this system is not well known for 4.2 °K. A linear variation in E_{gap} is shown in Fig. II-7, but this should be regarded as schematic. Both peak energies vary with composition in about the same manner as E_{gap}. Since the widths of the peaks remain essentially constant across the whole composition range, the trapping energy (which is the difference between E_{gap} and the high-energy side of the band) is essentially constant. This is expected on the basis of the isoelectronic trap model, since the trapping energy is determined primarily by the electronegativity difference between S and Te.

At 4.2 °K, the wavelength at the peak of band B changes from 7000 Å in the red to 4550 Å in the blue as the alloy composition changes from pure CdS to pure ZnS. The peak energy for a given composition does not depend strongly on temperature. Therefore, a similar range is observed at room temperature. Since the trapping energy is essentially constant, the fluorescent quantum efficiency over this whole range should be comparable to the high efficiency reported for CdS. This suggests that Te-doped CdS-ZnS alloys should be investigated as a possible source of efficient room temperature electroluminescence for most of the visible spectrum.

Luminescence data for Te-doped ZnS-ZnSe alloys at 4.2 °K are shown in Fig. II-8, where the photon energy at the peak of each band is plotted vs the mole fraction of ZnS. The variation in E_{gap} with composition is again shown schematically. In this alloy system, the peak energies are almost independent of alloy composition. Since the widths of the luminescence bands are almost constant, the trapping energy decreases strongly with decreasing ZnS. The energy of the trap responsible for the A-band luminescence becomes so small for alloys containing less than 25 mole percent ZnS that this luminescence is not observed at 4.2 °K in this composition range. This decrease in trapping energy with decreasing ZnS content is expected because Te and S differ more in electronegativity than do Te and Se.

For ZnS-ZnSe alloys doped with 0.5 atomic percent Te, the B-band is observed in samples which contain as little as 1 mole percent ZnS. This suggests that Te can act as an isoelectronic trap in ZnSe, even though the B luminescence is not observed in ZnSe which contains 0.5-atomic-percent Te but no S. To investigate this possibility, we measured the photoluminescence of pseudobinary ZnSe-ZnTe alloys. For alloys in which the mole fraction of ZnTe is between 0.03 and 0.5, a broad band in the neighborhood of 2.5 eV is observed at 4.2 °K. Figure II-9 shows the peak energy for this band plotted against the mole fraction of ZnTe. We believe that the band may be due to Te acting as an isoelectronic trap, although we cannot exclude the possibility that it results from an impurity present in the ZnTe.

G. W. Iseler
A. J. Strauss

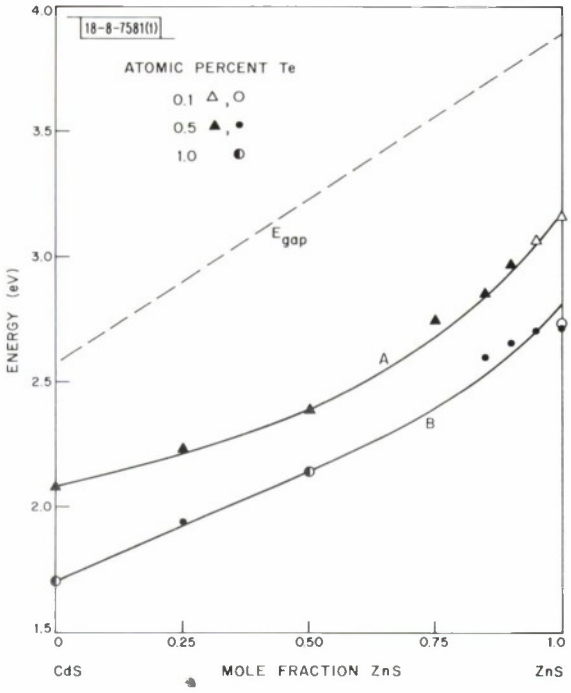

Fig. II-7. Photon energy at photoluminescence peoks due to isoelectronic Te traps in ZnS-CdS olloys, os o function of mole froction of ZnS.

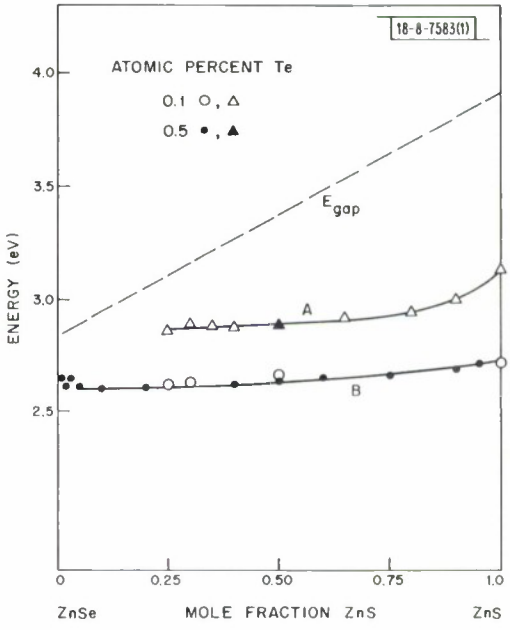

Fig. II-8. Photon energy at photoluminescence peaks due to isoelectronic Te traps in ZnS-ZnSe olloys, as a function of mole froction of ZnS.

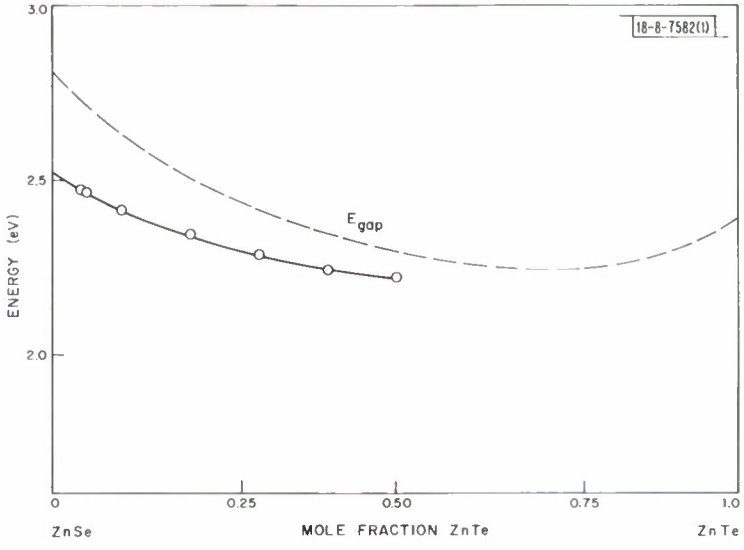

Fig. II-9. Photon energy ot photoluminescence peok in ZnSe-ZnTe olloys, as o function of mole froction of ZnTe.

D. STRUCTURAL, ELECTRICAL, AND MAGNETIC PROPERTIES OF VACANCY-STABILIZED CUBIC TiO AND VO

The cubic compounds TiO and VO have an extremely wide homogeneity range, with x in MO_x ranging from about 0.75 to 1.30. Both have the defect rock-salt structure, with a total vacancy content as high as 20 percent of the total lattice sites. Although these compounds have been studied extensively, each of the previous investigators has concentrated on only one or two properties, and many of the samples have been poorly characterized, with the result that the published data are inconsistent and incomplete.

Our investigation was undertaken to provide a consistent body of data on a large number of properties, measured on samples prepared and analyzed identically. We have made measurements of lattice parameter, density, resistivity, Seebeck coefficient, and magnetic susceptibility on many single-phase samples spanning the homogeneity range of each compound. Most of the samples were prepared as polycrystalline arc-melted buttons or arc-cast rods and then annealed at 1300° or 1500°C. Some samples of $VO_{1.3}$ were single crystals grown by the Czochralski method. The preparation and characterization of these materials are described in detail in Ref. 11.

For TiO, the lattice parameter a_o and density d both decrease linearly with increasing x. The data are in good agreement with the a_o values of Anderson, et al.,[12] and with the d values of Denker.[13] If it is assumed that the vacancies are randomly distributed among the lattice sites and that there are no atoms on interstitial sites, the fraction of cation sites filled is given by $f_c = da_o^3N/4(M + 16x)$, where M is the molecular weight of the metal and N is Avogadro's number. The fraction of oxygen sites filled is given by $f_o = xf_c$. The percentages of titanium and oxygen vacancies, $V_{Ti} = 100\ (1 - f_c)$ and $V_O = 100\ (1 - f_o)$, are plotted against x in Fig. II-10. Both V_{Ti} and V_O vary linearly with x. It is noteworthy that the oxygen vacancies go to zero at x = 1.30, the upper composition limit of the cubic phase, but the metal vacancies do not go to zero at the lower composition limit.

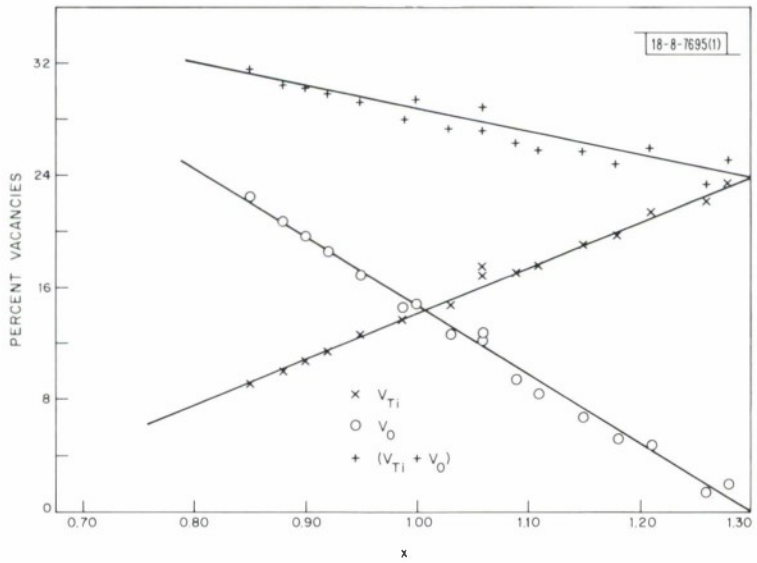

Fig. II-10. Percentage of titanium vacancies V_{Ti}, oxygen vacancies V_O, and total vacancies $(V_{Ti} + V_O)$ as a function of x for TiO annealed at 1300° or 1500°C at 1 atm.

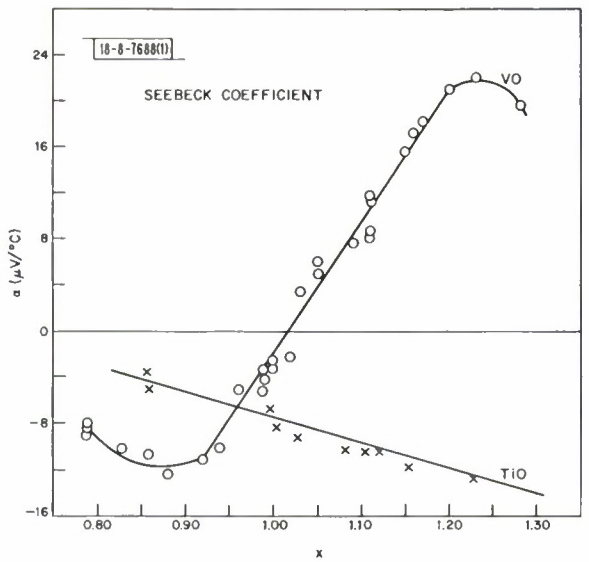

Fig. II-11. Absolute Seebeck coefficient α vs x for TiO ond VO.

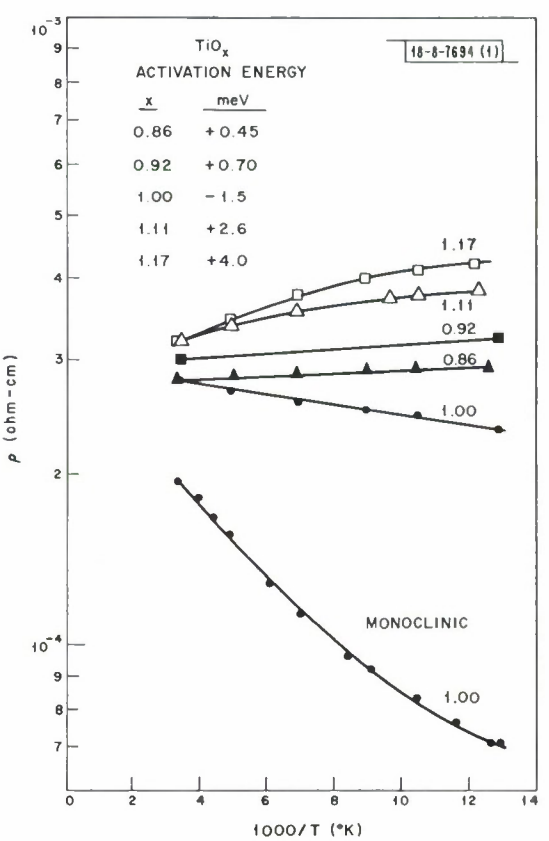

Fig. II-12. Resistivity ρ vs reciprocal temperoture for five compositions of cubic TiO ond for monoclinic $TiO_{1.00}$.

The Seebeck coefficient of TiO is negative, as shown in Fig. II-11. It changes with composition in an essentially linear manner from $-4\,\mu V/°C$ at x = 0.86 to $-12\,\mu V/°C$ at x = 1.24. The resistivity ρ vs temperature between 77° and 300°K is shown for five compositions of cubic TiO in Fig. II-12. The activation energy is negative only for compositions near x = 1.0, as reported by Denker.[13] This anomaly is probably due to incipient ordering during quenching, since only this composition can order without diffusion. To check this possibility, ρ was measured for a slice of the same ingot of $TiO_{1.00}$ which had been annealed at 900°C for 48 hours to convert it to the ordered monoclinic phase. The activation energy for this sample (Fig. II-12) is negative and even larger than that for the cubic sample, supporting the hypothesis of short range ordering in the latter.

No magnetic susceptibility was observed for TiO samples down to the limit of sensitivity of the vibrating-sample magnetomcter, $\chi_M \sim 150 \times 10^{-6}$. Ehrlich[14] has reported susceptibilities of about half this value.

The lattice parameters and densities of about 30 samples of VO are plotted against x in Fig. II-13. In contrast with TiO, a_o for VO increases with increasing x. The density of VO, like that of TiO, decreases linearly as x increases. At 1300°C, the lower limit of x for the cubic phase is between 0.75 and 0.79, and the upper limit is 1.28, on the basis of x-ray and metallographic examination of the annealed samples. Since x = 1.32 for one of the single crystals, $VO_{1.32}$ must be stable (or metastable) at the liquidus temperature. The percentages of V and O vacancies are plotted as a function of x in Fig. II-14 where the plots show a definite curvature. The oxygen sites are completely filled at the upper composition limit for annealed samples.

The resistivity of VO between 77° and 300°K is plotted in Fig. II-15. In agreement with the results of Kawano, et al.,[15] there is no discontinuity in the ρ vs 1/T curves as in those reported by Morin[16] and Austin.[17] Thus, our data fail to confirm the metal-semiconductor transition reported by the latter authors. Activation energies E_a calculated from the slopes of the straight-line portions of these curves at the higher temperatures are shown in Fig. II-16. The slope of E_a vs x increases sharply at x ~ 1.0. The relatively high values of E_a obtained for sufficiently oxygen-rich samples suggest that these materials are semiconductors over the entire temperature range investigated.

The thermoelectric power of VO is negative for x < 1.02 and positive for x > 1.02, as shown in Fig. II-11. The magnitude reaches a maximum of $-12\,\mu V/°C$ at x = 0.88 and $22\,\mu V/°C$ at x = 1.23.

The values of magnetic susceptibility χ_M of VO measured with increasing fields up to 17.2 kOe at 77° and 4.2°K show that at the higher temperature this compound is weakly paramagnetic over the entire composition range. The value of χ_M increases with increasing x at all temperatures from 4.2° to 273°K, as shown in Fig. II-17. At 273°K, the increase of χ_M with x is not very large, but at 4.2°K, χ_M increases by a factor of nearly 20 between x = 0.79 and 1.28.

Our data for χ_M as a function of temperature are in qualitative agreement with those of Kawano, et al.,[15] except that we did not see any evidence of the antiferromagnetic ordering which they observed at 4.6° and 10°K in samples with x = 1.15 and 1.26. Several samples in the range from x = 1.15 to 1.28 were examined carefully at temperatures from below 4.2° to 30°K in a vibrating coil magnetometer which had excellent temperature control and sensitivity. No evidence of a Néel point was found for any sample. Furthermore, since neither of the single crystals showed antiferromagnetic ordering down to 4.2°K, it is doubtful that this ordering exists for VO above this temperature.

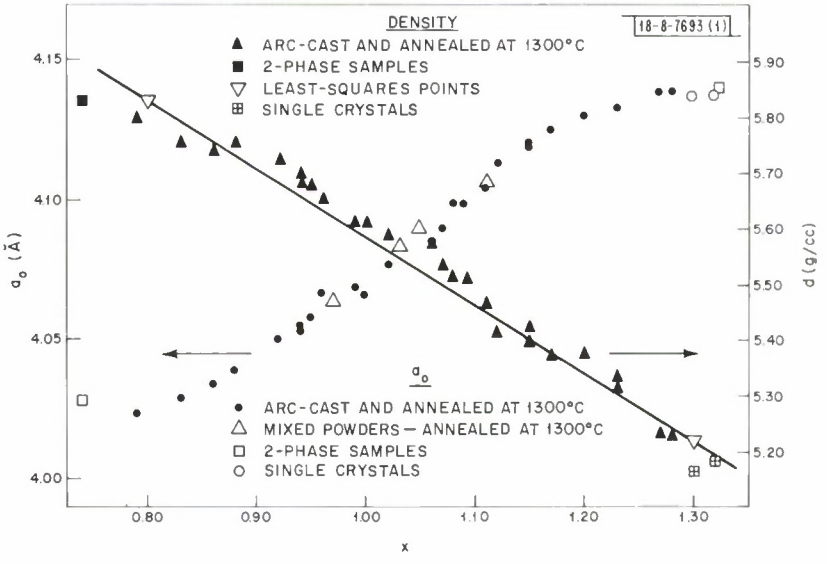

Fig. II-13. Lattice parameter a_o and density d vs x far VO.

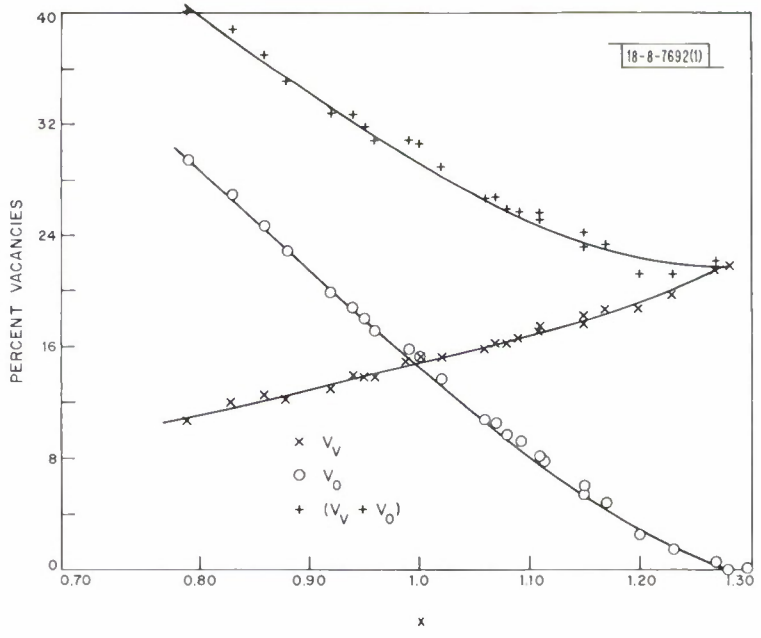

Fig. II-14. Percentage af vanadium vacancies V_V, axygen vacancies V_O, and tatal vacancies $(V_V + V_O)$ as a functian af x far VO annealed at 1300°C and 1 atm.

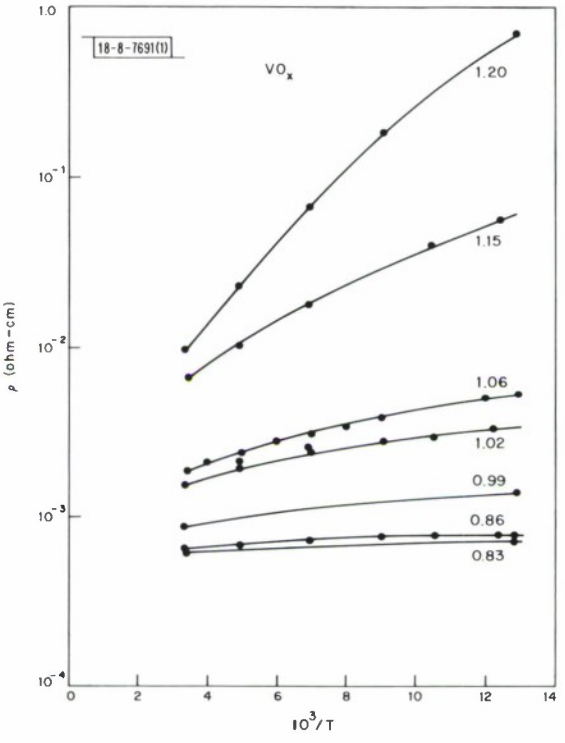

Fig. II-15. Resistivity vs reciprocal obsolute temperoture for seven compositians of VO.

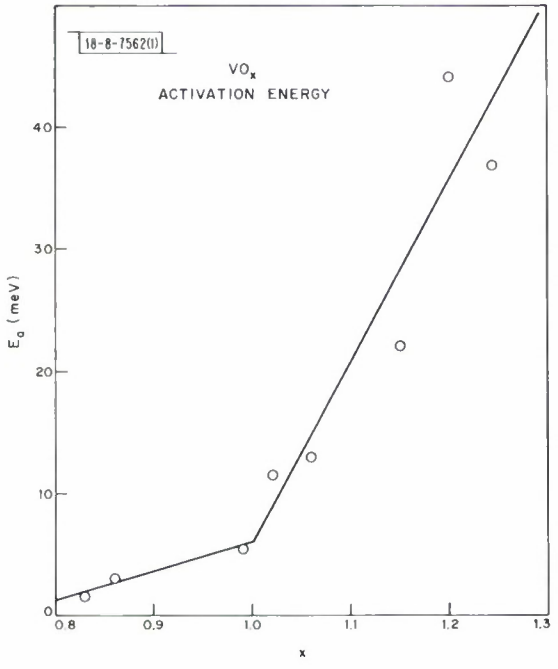

Fig. II-16. Activotian energy E_o vs x for VO.

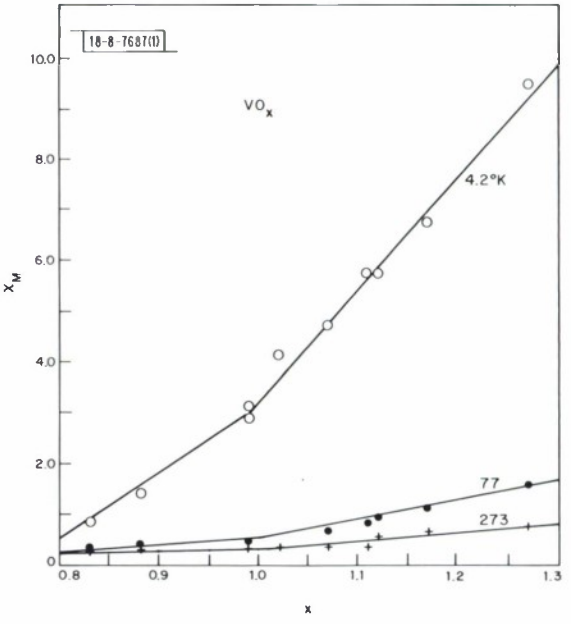

Fig. II-17. Molar susceptibility χ_M vs x for VO meosured ot 9.84 kOe with o vibroting somple magnetometer.

TABLE II-1

VO_x – EFFECT OF PRESSURE ON VACANCY CONCENTRATION

x	a_a (Å)		Density $(g/cc)^2$		Percent Vacancies $(V_V + V_O)$		Percent Decrease in Vacancies
	1 atm†	Pressure‡	1 atm†	Pressure‡	1 atm	Pressure	
0.86	4.034	4.047	5.736	5.816	37.0	33.2	−10.3
0.88	4.039	4.054	5.752	5.797	35.0	32.9	−6.0
0.94	4.053	4.066	5.677	5.732	32.7	29.4	−10.1
0.96	4.058	4.068	5.674	5.751	31.7	27.7	−13
0.99	4.068	4.084	5.602	5.650	30.8	27.7	−11
1.02	4.077	4.086	5.583	5.658	28.9	25.5	−12
1.09	4.099	4.104	5.507	5.581	25.7	22.5	−13
1.15	4.120	4.124	5.419	5.458	23.1	21.3	−8
1.20	4.130	4.133	5.371	5.402	21.3	19.9	−6.6
1.23	4.133	4.133	5.329	5.374	21.2	19.7	−7

† 1300°C and vacuum

‡ 1300°C and 60 kbars

In order to observe the effects of changing the number of vacancies in TiO and VO without changing the composition, samples of both were subjected to high-temperature annealing under pressures of 50 to 90 kbars, which removed an appreciable fraction of the vacancies, and then were re-examined. The effect of this pressure anneal on TiO has already been reported.[18] In the case of VO, the densities increased by an average of 1.0 percent, and the increase in a_o was about 0.1 percent, as shown in Table II-1. The decrease in vacancy content for VO was only 6 to 13 percent, compared with the reduction of 12 to 22 percent for TiO. It may actually be possible to remove all the vacancies from $TiO_{1.0}$ by annealing at higher pressure and temperature, as reported by Doyle, et al.[19] However, these authors do not give sufficient data to eliminate the possibility that their observed increase in a_o and decrease in vacancy content are due to impurities from the container or changes in oxygen content.

The decrease in vacancies on annealing at high pressure caused changes in the electrical and magnetic properties of both TiO and VO. The most notable change for TiO was the increase in the superconducting transition temperature reported earlier.[18] Another notable result for TiO was that the temperature coefficient of resistivity for samples with x = 1.0 changed from positive to negative, as for normal samples with other values of x. The Seebeck coefficient of both TiO and VO changed so that n-type samples had lower values, while the p-type VO samples had larger values. Due to pressure anneal, the Seebeck coefficient of $VO_{1.02}$ changed from negative to positive. Pressure anneal does not appreciably change the resistivity of VO samples.

The decrease in vacancies as a result of pressure does not change the magnetic susceptibility of VO to any great extent. At all compositions there is a 10- to 20-percent decrease in χ_M in the range from 4.2° to 100°K. For $x > 1.0$, this decrease is observed all the way to room temperature, but for $x < 1.0$ there appears to be no significant difference above 100°K. Thus, a decrease in anion vacancies caused by pressure has an effect on χ_M opposite to that observed when the decrease in vacancies is caused by increasing x. This indicates that the susceptibility is more sensitive to the cation vacancies than to the anion vacancies.

M. D. Banus T. E. Stack
T. B. Reed R. E. Fahey

E. HIGH-PRESSURE PHASES WITH PEROVSKITE-RELATED STRUCTURES IN THE SYSTEM $Sr_{1+x}IrO_{3+x}$

There is a large class of compounds with the general formula $A_{1+x}BX_{3+x}$ ($x = 0, \frac{1}{3}, \frac{1}{2}, 1$) which have a series of closely related structures, provided the large A-cation has a radius $1.0 < r_A < 1.9$ Å and the smaller B-cation has a radius $0.5 < r_B < 1.2$ Å. In the formula, X represents an anion such as oxygen, fluorine, or chlorine. The structures all consist of a number of perovskite units (ABX_3) interleaved with rock-salt layers (AX) that have a common c-axis with the body-centered tetragonal unit cell of this class of compounds. For ABX_3 ($x = 0$), there are only perovskite units [Fig. II-18(a)] and no rock-salt layers. For $A_4B_3X_{10}$ ($x = \frac{1}{3}$), three perovskite units alternate with a rock-salt layer [Fig. II-18(b)]; for $A_3B_2X_7$ ($x = \frac{1}{2}$), two perovskite units alternate with a rock-salt layer [Fig. II-18(c)]; and for A_2BX_4 ($x = 1$), one perovskite unit alternates with a rock-salt layer [Fig. II-18(d)].

In the system $Sr_{1+x}IrO_{3+x}$, the structure of the atmospheric pressure form of $SrIrO_3$ ($x = 0$) is closely related to the hexagonal modification of $BaTiO_3$ and does not fit into the four-member structural series just described. At 1000°C and 45 kbars, however, this compound transforms into the orthorhombic perovskite structure ($a = 5.58$ Å, $b = 5.60$ Å, $c = 7.89$ Å) which is the first member of the series.[20] The last member, Sr_2IrO_4 ($x = 1$), is formed at atmospheric pressure.[21] The intermediate members of the series, $Sr_4Ir_3O_{10}$ ($x = \frac{1}{3}$) and $Sr_3Ir_2O_7$ ($x = \frac{1}{2}$), have not been prepared previously. We have now synthesized both of these compounds at high pressure by reacting appropriate quantities of Sr_2IrO_4 and IrO_2 at 1000°C. The compound $Sr_4Ir_3O_{10}$, with tetragonal cell dimensions $a = 3.93$ Å and $c = 28.4$ Å, is formed at pressures exceeding 35 kbars; $Sr_3Ir_2O_7$, with tetragonal cell dimensions $a = 3.90$ Å and $c = 20.90$ Å, is formed at pressures greater than 10 kbars.

The syntheses were performed in a high-pressure belt apparatus capable of developing pressures to 90 kbars. In a typical run, the platinum encapsulated specimen was subjected to the desired pressure, after which the temperature was raised to 1000°C and held for one-half hour. The specimen was then quenched to room temperature before the pressure was released. Structural analysis of the products obtained was carried out at atmospheric pressure with a Norelco x-ray powder diffractometer with vertical goniometer.

At temperatures above 800°C, the high-pressure phases $Sr_3Ir_2O_7$ and $Sr_4Ir_3O_{10}$ slowly decompose to $SrIr_2O_4$. Even at 1200°C, the perovskite form of $SrIrO_3$ only slowly retransforms to its atmospheric pressure form.

J. M. Longo T. W. Hilton
J. A. Kafalas D. A. Batson

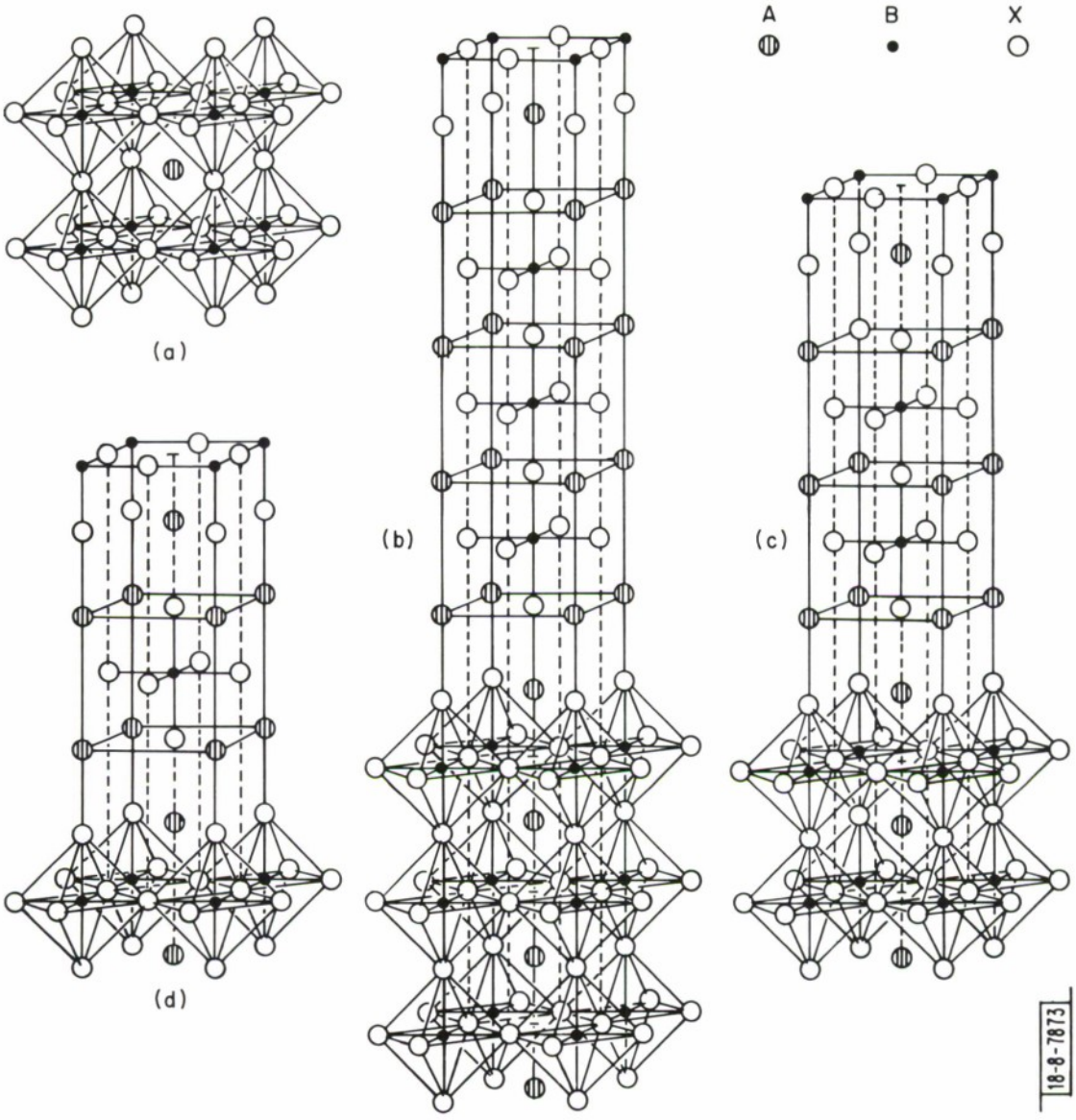

Fig. II-18. Structures of compounds in $A_{1+x}BX_{3+x}$ series: (a) ABX_3 (x = 0); (b) $A_4B_3X_{10}$ ($x = \frac{1}{3}$); (c) $A_3B_2X_7$ ($x = \frac{1}{2}$); (d) A_2BX_4 (x = 1).

REFERENCES

1. R. F. Bis and J. R. Dixon, Bull. Am. Phys. Soc. 13, 1394 (1968).
2. S. S. Devlin in Physics and Chemistry of II-VI Compounds, M. Aven and J. S. Prener, eds. (John Wiley and Sons, Inc., New York, 1967), p. 551.
3. W. W. Piper and S. J. Polich, J. Appl. Phys. 32, 1278 (1961).
4. M. Aven and B. Segall, Phys. Rev. 130, 1 (1963).
5. M. R. Lorenz in Physics and Chemistry of II-VI Compounds, M. Aven and J. S. Prener, eds. (John Wiley and Sons, Inc., New York, 1967), p. 85.
6. Y. Fukuda and M. Fukai, J. Phys. Soc. Japan 23, 902 (1967).
7. M. Aven and H. H. Woodbury, Appl. Phys. Letters 1, 3 (1962).
8. D. G. Thomas, Phys. Soc. Japan 21 (Supp.), 265 (1966).
9. J. D. Cuthbert and D. G. Thomas, J. Appl. Phys. 39, 1573 (1968).
10. G. W. Iseler and A. J. Strauss, Bull. Am. Phys. Soc. 13, 404 (1968).
11. M. D. Banus and T. B. Reed, Proceedings of the Institute on Extended Defects in Non-metallic Solids, Phoenix, 1969 (to be published).
12. S. Anderson, B. Collén, U. Kuylenstierna, and A. Magnéli, Acta Chem. Scand. 11, 1641 (1957).
13. S. P. Denker, Ph. D. Thesis, Department of Electrical Engineering, M. I. T. (1963).
14. P. Ehrlich, Z. Elektrochem. 45, 362 (1939).
15. S. Kawano, K. Kasuge, and S. Kachi, J. Phys. Soc. Japan 21, 2744 (1966).
16. F. J. Morin, Phys. Rev. Letters 3, 34 (1959).
17. I. G. Austin, Phil. Mag. 7, 961 (1962).
18. Solid State Research Report, Lincoln Laboratory, M. I. T. (1967:2), p. 24, DDC 656548, H-853; Mat. Res. Bull. 3, 723 (1968), DDC 677839.
19. N. J. Doyle, J. K. Hulm, C. K. Jones, R. C. Miller, and A. Taylor, Phys. Letters 26A, 604 (1968).
20. Solid State Research Report, Lincoln Laboratory, M. I. T. (1968:3), p. 33, DDC 678534, H-899.
21. J. J. Randall, L. Katz, and R. Ward, J. Amer. Chem. Soc. 79, 266 (1957).

III. PHYSICS OF SOLIDS

A. MAGNETISM

1. Spin Splittings in Reflectivity of Ferromagnetic EuO†

We have continued our study of the band structure of the magnetic semiconductor EuO by examining the effects of ferromagnetic ordering on the reflectivity spectrum at energies above the absorption edge. The reflectivity was studied from 0.5 to 5.2 eV and at several fixed temperatures from 1.5 °K through the Curie point at 69 °K and above. Figure III-1 shows that the peak E_1 at 1.5 eV, which is associated with the absorption edge, has an anomalously large red-shift on cooling through the Curie point. This shift is similar to the absorption edge red-shift,[1] but is not quite so big.

In addition to the temperature shift, E_1 was observed to broaden below 40 °K; at the lowest temperatures, a second peak (E_1') was resolved as it split off from E_1 and moved to lower energy.

A second peak, E_2 at 4.65 eV, was also studied as a function of temperature. As seen in Fig. III-1, E_2 does not appear to have a red-shift. However, at low temperatures this peak appears to split into two shoulders and develops a remarkably sharp peak at 4.95 eV.

In a second set of experiments, the E_1 peak was studied at two fixed temperatures, 1.5 ° and 70 °K, with circularly polarized light and a domain-orienting magnetic field of 42 kOe. The results given in Fig. III-2 indicate that (near T_c) E_1 is resolved into left and right circularly polarized components of a doublet with a separation of 0.25 eV. With full magnetic saturation at 1.5 °K, the doublet develops into a triplet with left and right circularly polarized extrema E_1'' and E_1', respectively, and a mixed central component E_1. The extrema are each separated from the central peak by 0.25 eV.

We have analyzed these data in the light of most recent measurements of the spectrum of Eu^{2+} in other compounds[2] and have developed an energy level scheme which appears consistent with the data. In this model, the E_1 and E_2 reflectivity structures arise from a transition from the localized $4f^7$ ground state of the Eu^{2+} ion to a final state consisting of a $4f^6$ excited state and an electron in one of the spin-split components of the 5d-band. The different J components of the $4f^6$ manifold give rise to a doublet in E_1 near T_c which then becomes further split by the exchange splitting of the t_{2g} component of the 5d-band at low temperatures. The E_2 peak shows a ladder structure due to these transitions which involve the e_g component of the d-band. We believe that the behavior of E_1 gives the first direct optical evidence for a spin-split conduction band. A report on this work has been submitted for publication.

J. Feinleib
W. J. Scouler
J. O. Dimmock
J. Hanus
T. B. Reed
C. R. Pidgeon‡

† Part of thia work was carried out at the Francis Bitter National Magnet Laboratory, M.I.T.

‡ Francis Bitter National Magnet Laboratory, M.I.T.

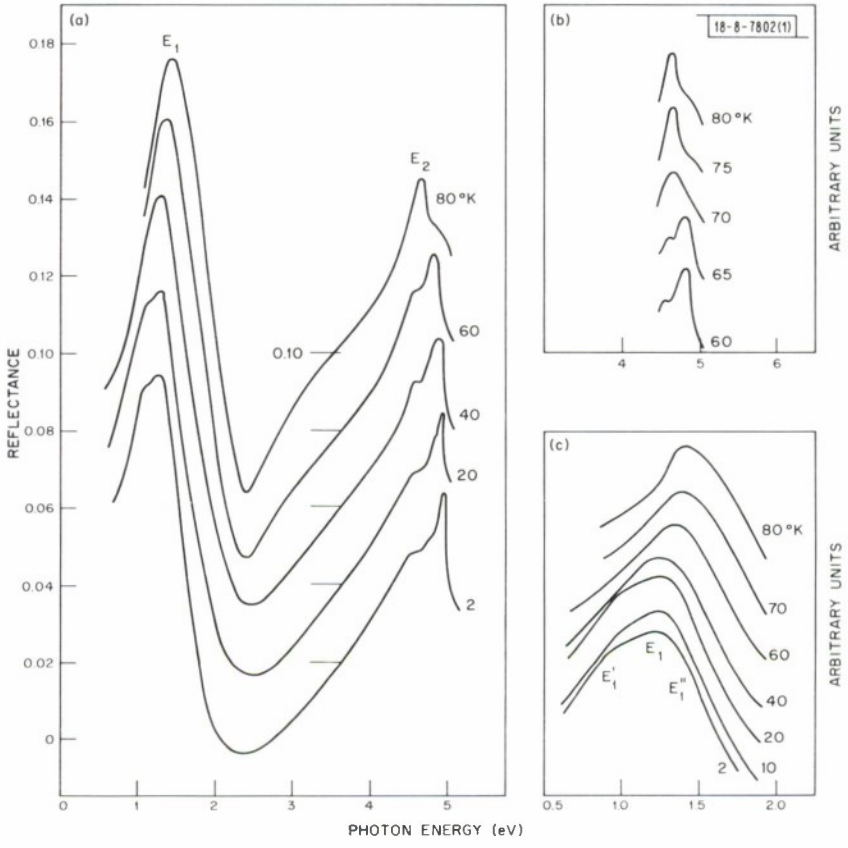

Fig. III-1. (a) Reflectance vs phatan energy at selected temperatures abave and belaw Curie paint, $T_c = 69°K$. Each curve is arbitrarily displaced 0.02 eV fram ane abave. (b) Details af E_2 near T_c. (c) Details af E_1.

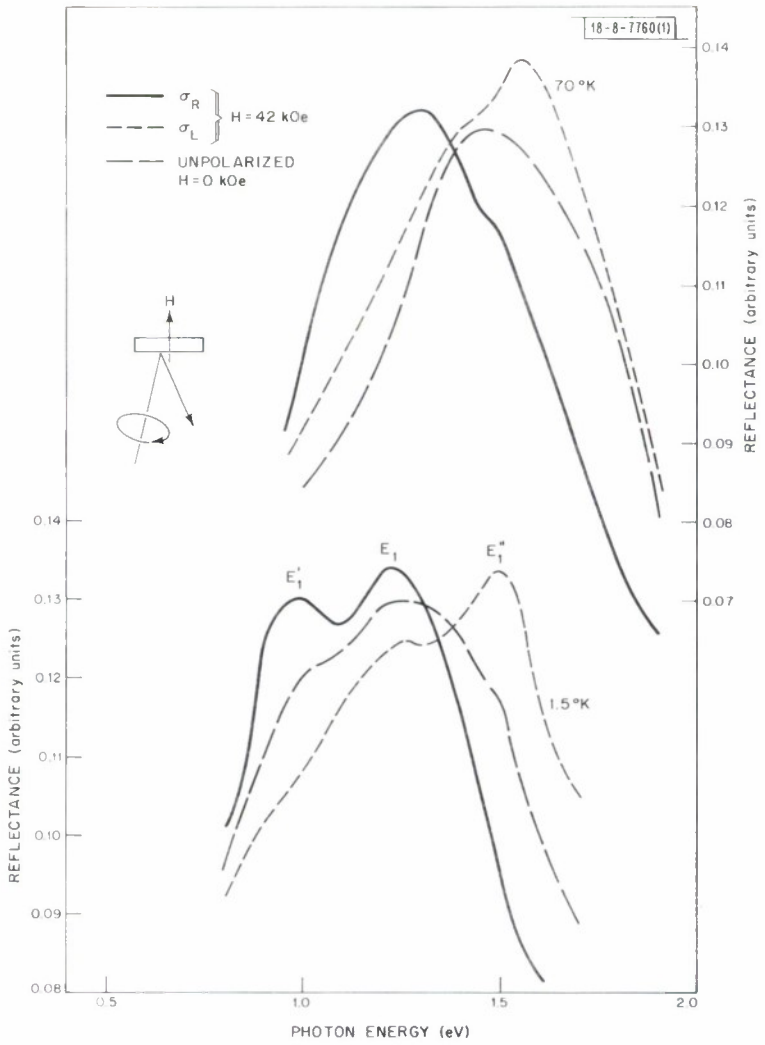

Fig. III-2. Reflectonce vs photon energy for right ond left circulorly polarized light ot 70° and 1.5°K. Unpolarized reflectance is olso shown.

2. Magnetic Properties of $CoS_{2-x}Se_x$

CoS_2 exhibits metallic conductivity and is ferromagnetic below $T_c \simeq 120°K$. It is of considerable theoretical interest because it appears to be an example of narrow d-band ferromagnetism without the usual complication of a broad overlapping s-band.[3] Johnson[4] has investigated the effect of partial substitution of selenium for sulfur in the system $CoS_{2-x}Se_x$ over the entire range $0 < x < 2$ and found that increasing x decreased T_c and led to a sharper ferromagnetic transition. The saturation moment per cobalt ion remained approximately constant up to $x = 0.20$. For $x > 0.20$, the saturation moment per cobalt ion decreased rapidly and the system became antiferromagnetic for $x > 0.30$.

In order to gain additional insight into the nature of the magnetic interactions, we have initiated a further investigation of this system, with particular emphasis on the magnetic transition region. Preliminary measurements on a sample of $CoS_{1.8}Se_{0.2}$ in the remanent field ($H \cong 65$ Oe) of the electromagnet showed the existence of a transition at 50°K. However, a similar measurement carried out in a field of 10 kOe showed the transition to be equally sharp, but with a transition temperature of 55.5°K. This behavior could be indicative of a first-order transition rather than the second-order transition normally observed at the Curie temperature. A more complete study of the effect of magnetic field on the transition temperature was conducted on $CoS_{1.9}Se_{0.1}$, with the results shown in Fig. III-3. The diffuseness of the transition temperature, even in the

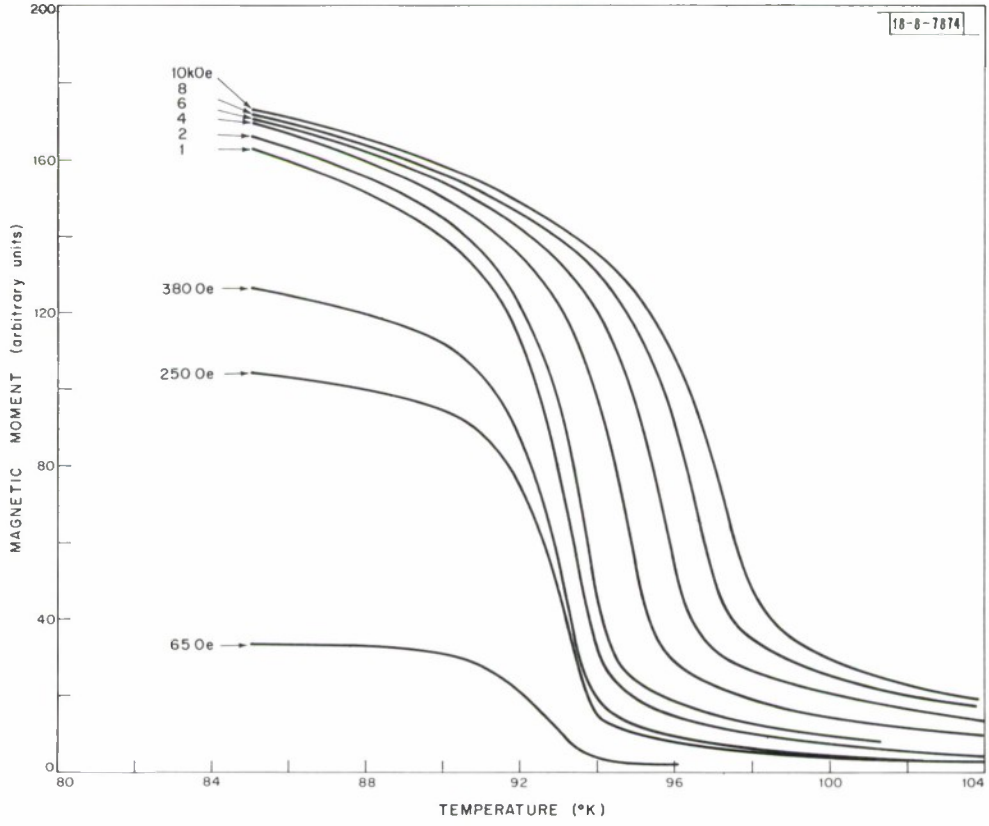

Fig. III-3. Magnetic moment vs temperature in $CoS_{1.9}Se_{0.1}$ at various applied fields in vicinity of transition temperature.

lowest fields, indicated the presence of inhomogeneity in the sample composition. However, it is seen that the major effect of the applied field is to raise the transition temperature, giving rise to apparent metamagnetic behavior in the temperature interval which falls above the transition at lowest fields and below the transition at the highest fields (i. e., between 94° and 96°K in Fig. III-3). No temperature hysteresis was observed on cooling and warming through the transition.

A study of the effect of pressure on the transition temperature was made between atmospheric pressure and 10 kbars both in the remanent field and at 10 kOe. The pressure dependence was found to be linear and independent of field over this pressure range, being equal to -1.06 (± 0.03) deg/kbar at remanence and -1.02 (± 0.03) deg/kbar at 10 kOe. Thus, within experimental accuracy, the pressure dependence of the transition temperature $(\partial T_t/\partial p)_H$ is a constant and independent of applied field; similarly, the field dependence $(\partial T_t/\partial H)_p$ is approximately constant and independent of pressure.

Assuming a first-order transition, the Clausius-Clapeyron equation

$$\left(\frac{dT_t}{dH}\right)_p = -\frac{\Delta M}{\Delta V}\left(\frac{dT_t}{dp}\right)_H \qquad \text{(III-1)}$$

requires that, for constant $(dT_t/dH)_p$ and $(dT_t/dp)_H$, the change in volume ΔV on going through the transition be proportional to the change in magnetization ΔM. Since the magnetization change through the transition at H = 10 kOe is approximately four times greater than ΔM at H = 65 Oe, this implies that the volume change at 10 kOe is four times as great as that at 65 Oe. This is reasonable only if the volume change is extremely small through the transition. Alternatively, assuming a second-order phase change at the transition, we find the variation of magnetic moment with pressure at 55°K to be consistent with the experimental value of dT_t/dp. Regarding the order of the phase transition, these results raise numerous questions which we hope to resolve by means of differential thermal analysis.

Since the start of our investigation, a series of papers on this system has been published by Adachi and co-workers.[5-7] Where measurements overlap, they are in essential accord, except for the pressure dependence of the CoS_2 Curie point; Adachi, et al., find a value of -0.86 deg/kbar compared with our value (reported at the recent magnetism conference[8]) of -0.6 deg/kbar. However, the critical feature is that we both observe a decrease in T_c with decreasing size. Since the substitution of Se for S into the system increases the lattice size, it is apparent that the concurrent decrease in Curie point is not a size effect.

Hattori, Adachi, and Nakano[7] explained their results on the basis of ferromagnetic nearest-neighbor (J_1) and antiferromagnetic next-nearest-neighbor (J_2) interactions. Utilizing the high-temperature expansion technique and truncating the series after three terms, they concluded that the material orders antiferromagnetically for $J_2/J_1 < -0.24$ and ferromagnetically, with a first-order transition, for $J_2/J_1 \approx -0.20$. Since the fcc structure has 12 nearest neighbors and only 6 next-nearest neighbors, the above results seemed physically unreasonable to us. We therefore investigated (see Sec. 3 below) the ground-state configuration of the fcc lattice with nn and nnn interactions; from our results, we concluded that for ferromagnetic nn and antiferromagnetic nnn interactions the ground state does not become antiferromagnetic until $J_2/J_1 < -1$.

We believe the major source of the discrepancy between our result and that of Hattori, et al.,[7] lies in the uncertainties involved in the truncation of their series expansion after evaluating three terms. This is further borne out by the conclusions of Wood and Dalton[9] who studied the high-temperature expansion of the zero-field susceptibility in the fcc structure with nn and nnn interactions to fifth order. They found that the convergence of the series is extremely poor for $S = \frac{1}{2}$ and $\alpha < 0$ (the case corresponding to $CoS_{2-x}Se_x$ over the range considered above).

N. Menyuk J. A. Kafalas
K. Dwight A. Wold†

3. Ground State Spin Configuration in Face-Centered-Cubic Lattice

A study has been made in the $CoS_{2-x}Se_x$ system of the spin configuration which minimizes the classical Heisenberg exchange energy in the fcc lattice with first- and second-neighbor interactions. Taking $\vec{S}_i$ as the spin at position $\vec{R}_i$, we find the energy is

$$E = J_1 \sum_{i,j} \vec{S}_i \cdot \vec{S}_j + J_2 \sum_{k,\ell} \vec{S}_k \cdot \vec{S}_\ell \qquad \text{(III-2)}$$

where J_1 and J_2 are the first- and second-nearest-neighbor interactions, respectively. Negative and positive values of J correspond to ferro- and antiferromagnetic interactions, respectively. Since the fcc is a Bravais lattice, all the sites are equivalent, in which case Lyons and Kaplan[10] have shown that the ground state configuration is always a simple spiral, involving a single wave vector $\vec{k}$.

Expressing the spins as $\vec{S}_i = S \exp[i\vec{k} \cdot \vec{R}_i]\,\hat{\sigma}_i$, where $\hat{\sigma}_i$ is a unit vector in the direction of $\vec{S}_i$ and $S = |\vec{S}_i|$, Eq. (III-2) becomes

$$\frac{E}{2J_1S^2} = \sum_{\vec{R}_i - \vec{R}_j} \exp[i\vec{k} \cdot (\vec{R}_i - \vec{R}_j)] + \alpha \sum_{\vec{R}_k - \vec{R}_\ell} \exp[i\vec{k} \cdot (\vec{R}_k - \vec{R}_\ell)] \qquad \text{(III-3)}$$

where $\alpha = J_2/J_1$. Finding the minimum energy solution of Eq. (III-2) then reduces to the problem of finding the value of $\vec{k}$, which minimizes the left-hand side of Eq. (III-3) for positive J_1 and maximizes it for negative J_1. For the fcc structure, Eq. (III-3) can be rewritten as

$$\frac{E}{2J_1S^2} = 2J_1\{2\cos\pi h \cos\pi k + 2\cos\pi k \cos\pi\ell + 2\cos\pi\ell \cos\pi h + \alpha[\cos 2\pi h + \cos 2\pi k + \cos 2\pi\ell]\} \qquad \text{(III-4)}$$

where $\vec{k} = (2\pi/a)(h\hat{i} + k\hat{j} + \ell\hat{k})$. It can be shown that the possible values of h, k, and ℓ which can minimize the energy are limited to the sets: (0, 0, 0), (0, 0, 1), $(1, \frac{1}{2}, 0)$, (1, 1, 0), $(\frac{1}{2}, \frac{1}{2}, \frac{1}{2})$, (1, 1, 1), and (0, 0, ℓ), with $\cos\pi\ell = -(1/\alpha)$ thereby restricting α to $|\alpha| > 1$; and (h, h, 0), with $\cos\pi h = -[1/(1 + 2\alpha)]$ thereby restricting α to the regions $\alpha < -1$ and > 0. Of the above sets, (1, 1, 1) and (0, 0, 0) are equivalent and correspond to ferromagnetism, while the (0, 0, 1) and (1, 1, 0)

† Brown University, Providence, Rhode Island.

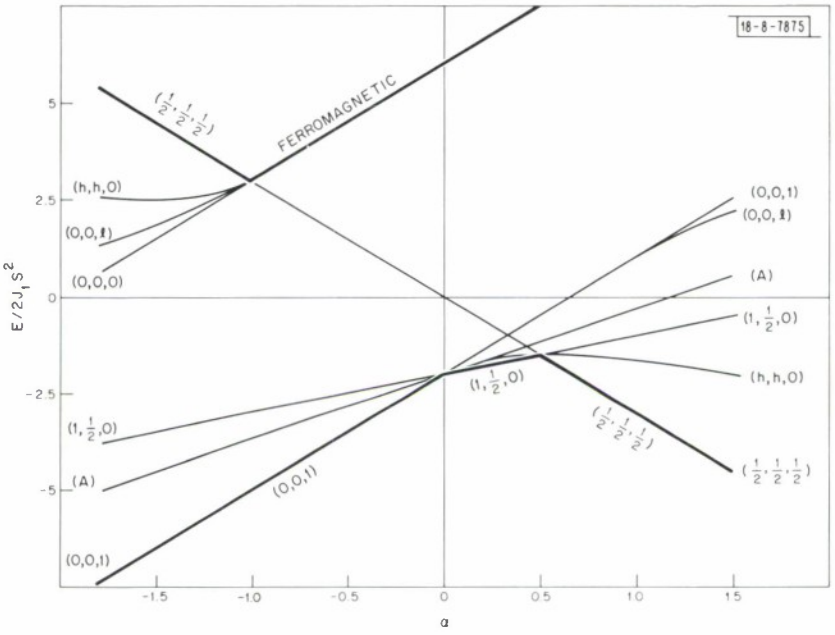

Fig. III-4. $E/2J_1S^2$ vs α for all possible sets in the fcc lattice. Heavy lines correspond to energy minima and are labeled.

are also equivalent and correspond to ordering of the first kind.[11] The $(\frac{1}{2}, \frac{1}{2}, \frac{1}{2})$ and $(1, \frac{1}{2}, 0)$ correspond to ordering of the second and third kind, respectively.[11] The value of $E/2J_1S^2$ as obtained from Eq. (III-4) is plotted in Fig. III-4 as a function of α for all the possible sets. It can be seen that only $\vec{k} = 0$, $(0, 0, 1)$, $(\frac{1}{2}, \frac{1}{2}, \frac{1}{2})$, and $(1, \frac{1}{2}, 0)$ ever represent energy extrema,† corresponding to ferromagnetism or collinear antiferromagnetic order of the first, second, or third kind, respectively.

The regions in the J_1-J_2 interaction space in which each of these is a minimum is shown in Fig. III-5. It can be seen that for a ferromagnetic (negative) J_1, the ground state will be ferromagnetic unless $\alpha < -1$, in contrast with the results of Hattori, et al.[7]

Adachi, et al.,[5] investigated the spin configurations of CoSSe and $CoSe_2$ by neutron diffraction. They were able to obtain agreement with their diffraction pattern by assuming a configuration which corresponds to none of the above and which cannot be expressed by using a single $\vec{k}$ vector. According to Lyons and Kaplan,[10] it can therefore never have the lowest energy within the Heisenberg model. We have evaluated the energy of the Adachi, et al.,[5] configuration and this is plotted in Fig. III-4 as the line labeled A; as predicted, it is a higher energy configuration. Therefore, if the configuration assigned by Adachi, et al., is correct, there must be significant contributions to the energy from sources other than the Heisenberg interactions in these materials.

N. Menyuk
K. Dwight

† We have used the shorthand notation $(hk\ell)$ to correspond to $(2\pi/a)(h\hat{i} + k\hat{j} + \ell\hat{k})$.

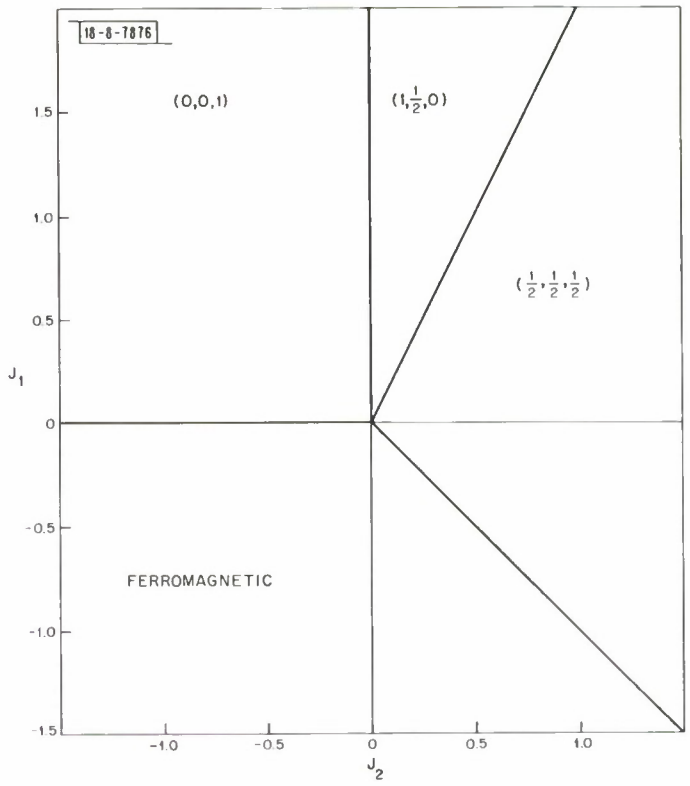

Fig. III-5. J_1 vs J_2 in fcc lattice showing regions in which lobeled configurations represent minimum energy. (0,0,1) corresponds to ordering of first kind, $(\frac{1}{2},\frac{1}{2},\frac{1}{2})$ to ordering of second kind, ond $(1,\frac{1}{2},0)$ to ordering of third kind.

4. Spin Configurations in Normal Cubic Spinels

The original treatment of spin configurations in normal cubic spinels by Lyons, Kaplan, Dwight, and Menyuk[12] was restricted to consideration of nearest-neighbor A-B and B-B exchange interactions, J_{AB} and J_{BB}. They discovered a low-energy spin configuration having the form of a conical spiral:

$$\hat{S}_{m\mu} = \sin\varphi_\mu[\hat{x}\cos(\vec{k}_o\cdot\vec{R}_{m\mu}+\gamma_\mu)+\hat{y}\sin(\vec{k}_o\cdot\vec{R}_{m\mu}+\gamma_\mu)]+\hat{z}\cos\varphi_\mu \qquad \text{(III-5)}$$

where m specifies the unit cell, μ identifies the site within the unit cell, $\vec{k}_o = (h_o, h_o, 0)$, and φ_μ and h_o are functions of the parameter $u = 4\bar{J}_{BB}/3\bar{J}_{AB}$ where the spin magnitudes have been incorporated into the exchange interactions, i. e., $\bar{J}_{AB} = J_{AB}S_AS_B$. This spiral had lower energy than either the Néel or Yafet-Kittel configurations when $u > 8/9$, and gave good agreement with many of the observed properties of $CoCr_2O_4$ when the value $u \cong 2$ was assumed.[13]

Subsequently, we investigated the effects of distant-neighbor B-B interactions upon the spin configuration in spinels having nonmagnetic A-site ions.[14] In particular, we found these distant interactions to be significant in determining the ground state of $ZnCr_2Se_4$, and arrived at estimates of their magnitudes from comparison with experiment. The strongest was $\bar{J}_{n\mu,\,m\mu} = \bar{U}\,\bar{J}_{BB'}$ which is the interaction between nearest neighbors <u>within</u> a given crystallographic sublattice.

These additional interactions should also be present when the A-sites contain magnetic ions. Therefore, we recently recomputed the minimum-energy conical spirals, including all these

distant-neighbor B-B interactions, and also including a nearest-neighbor A-A interaction.[15] This recalculation led to significant improvement in the agreement between theory and experiment for $CoCr_2O_4$, and for the first time provided an explanation for the kink in the observed variation of magnetization with temperature. From comparison with experiment, we then obtained revised estimates of $u \cong 1.7$ and $\overline{U} \cong 0.05$ for $CoCr_2O_4$.

However, Lyons, et al.,[12] showed their conical spiral to be locally unstable for values of u greater than 1.298. Consequently, it was surprising that the spins in $CoCr_2O_4$ should appear to form a spiral similar to that computed for $u = 2$. The reduction in the estimated value of u and the close agreement with experiment which resulted from the inclusion of distant-neighbor interactions (particularly $\overline{U}$) suggested that their inclusion might have increased the range of spiral stability. We have now investigated this attractive possibility, and find the opposite to be true.

Lyons, et al.,[12] showed that instability of the conical spiral corresponds to the existence of negative eigenvalues of the 12×12 matrix $M(\vec{k})$, where†

$$M^{\eta\eta}_{\nu\mu}(\vec{k}) = \frac{1}{2}[\Gamma_{\nu\mu}(\vec{k}) + \Gamma^{*}_{\nu\mu}(-\vec{k})] + \delta_{\nu\mu}H_{\nu}$$

$$M^{\xi\xi}_{\nu\mu}(\vec{k}) = \cos\varphi_{\mu}\cos\varphi_{\mu}M^{\eta\eta}_{\nu\mu}(\vec{k}) + \sin\varphi_{\nu}\sin\varphi_{\mu}[L_{\nu\mu}(\vec{k}) + \delta_{\nu\mu}H_{\nu}]$$

$$M^{\xi\eta}_{\nu\mu}(\vec{k}) = \frac{i}{2}\cos\varphi_{\nu}[\Gamma_{\nu\mu}(\vec{k}) - \Gamma^{*}_{\nu\mu}(-\vec{k})] = M^{\eta\xi *}_{\mu\nu}(\vec{k})$$

and

$$\Gamma_{\nu\mu}(\pm\vec{k}) = L_{\nu\mu}(\vec{k}_{o} \pm \vec{k})\exp[i(\gamma_{\mu} - \gamma_{\nu})]$$

$$L_{\nu\mu}(\vec{k}) = \Sigma_{m}\overline{J}_{n\nu,\,m\mu}\exp[i\vec{k}\cdot(\vec{R}_{m\mu} - \vec{R}_{n\nu})]$$

$$H_{\nu} = |\Sigma_{m\mu}\overline{J}_{n\nu,\,m\mu}\hat{S}_{m\mu}| \quad . \tag{III-6}$$

We have determined the maximum value of u, given various values for the other six exchange parameters, for which no matrix $M(\vec{k})$ defined above has a negative eigenvalue (for any k in the first Brillouin zone). The calculation was performed in double precision using an IBM 360/67 computer, and it involved a very precise determination of the equilibrium values for the δ_{μ}, H_{μ}, and k_{o}. We find the spiral instability boundary to be quite sensitive to $\overline{U}$, and insensitive to the other distant-neighbor interactions. Hence, the u-$\overline{U}$ plane depicted in Fig. III-6 contains the essence of our results – the conical spiral is unstable in the region of experimental interest.

The fact that the instability boundary of the conical spiral shown in Fig. III-6 intersects the boundary of the collinear Néel configuration is of particular significance. We have verified that, on both sides of this intersection, the Néel state is destabilized by spin deviations which possess nonzero Fourier components only for $\vec{k} = (h_{o}, h_{o}, 0)$, $(h_{o}, -h_{o}, 0)$, $(h_{o}, 0, h_{o})$, etc., where the value of h_{o} varies along the Néel boundary. As shown in Fig. III-6, the conical spiral, which is the unique spin configuration that can be constructed from just three Fourier components associated with $\vec{k} = 0, \pm(h, h, 0)$, is unstable for $\overline{U} > 0.052$. Hence, for $\overline{U} > 0.052$ there must exist

† Equations (D5) in Ref. 12 contain some typographical errors. The correct equations are presented here.

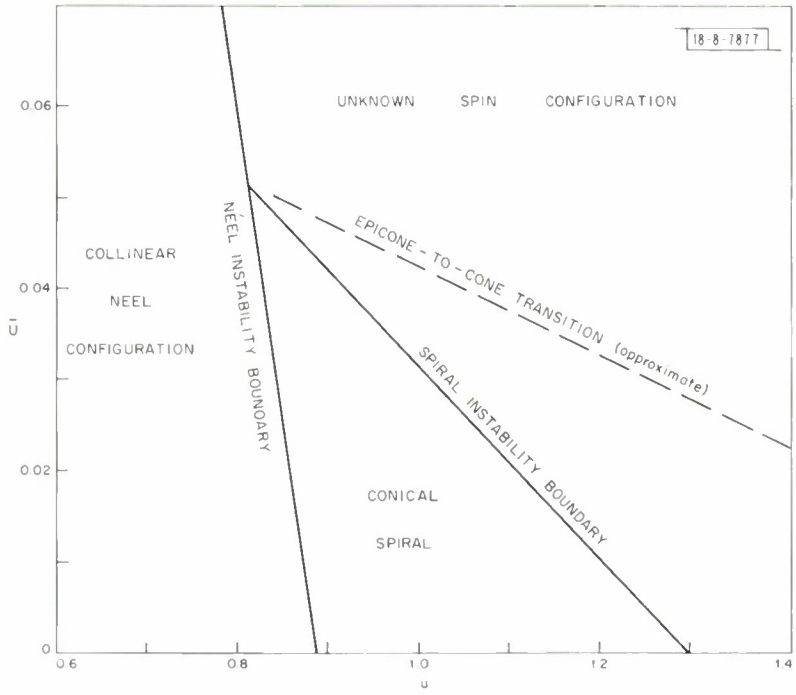

Fig. III-6. Instability boundaries in u-$\bar{U}$ plane.

some other, heretofore unimagined configuration which contains additional Fourier components associated with other members of the (h, h, 0) family.

Let

$$\hat{S}_{m\mu} = \sum_{\vec{k}} \vec{Q}_\mu(\vec{k}) \exp[i\vec{k} \cdot \vec{R}_{m\mu}] \tag{III-7}$$

and let $\vec{Q}_\mu(0)$, $\vec{Q}_\mu(\vec{k}_1)$, and $\vec{Q}_\mu(\vec{k}_2)$ all be nonzero. We have found that, when $\vec{k}_1$ and $\vec{k}_2$ are general $\vec{k}$'s (not equal to $\frac{1}{2}$ or $\frac{1}{3}$ of a reciprocal lattice vector), the constraining condition that

$$\hat{S}_{m\mu} \cdot \hat{S}_{m\mu} = 1 \tag{III-8}$$

cannot be satisfied unless either (a) both $\vec{Q}_\mu(\vec{k}_1 + \vec{k}_2)$ and $\vec{Q}_\mu(\vec{k}_1 - \vec{k}_2)$ are nonzero, or else (b) many other Fourier components are present. In case (a) there are further restrictions which lead to the unique solution

$$\begin{aligned}
\hat{S}_{m\mu} = {} & \hat{z}\{\cos\varphi_\mu \cos\varphi'_\mu - \sin\varphi_\mu \sin\varphi'_\mu \cos[\vec{k}_2 \cdot \vec{R}_{m\mu} + \gamma'_\mu]\} + \cos\varphi'_\mu \sin\varphi_\mu \\
& \times \{\hat{x} \cos[\vec{k}_1 \cdot \vec{R}_{m\mu} + \gamma_\mu] + \hat{y} \sin[\vec{k}_1 \cdot \vec{R}_{m\mu} + \gamma_\mu]\} + \tfrac{1}{2} \sin\varphi'_\mu (\cos\varphi_\mu + 1) \\
& \times \{\hat{x} \cos[(\vec{k}_1 + \vec{k}_2) \cdot \vec{R}_{m\mu} + (\gamma_\mu + \gamma'_\mu)] + \hat{y} \sin[(\vec{k}_1 + \vec{k}_2) \cdot \vec{R}_{m\mu} + (\gamma_\mu + \gamma'_\mu)]\} \\
& + \tfrac{1}{2} \sin\varphi'_\mu (\cos\varphi_\mu - 1) \{\hat{x} \cos[(\vec{k}_1 - \vec{k}_2) \cdot \vec{R}_{m\mu} + (\gamma_\mu - \gamma'_\mu)] \\
& + \hat{y} \sin[(\vec{k}_1 - \vec{k}_2) \cdot \vec{R}_{m\mu} + (\gamma_\mu - \gamma'_\mu)]\} \quad .
\end{aligned} \tag{III-9}$$

The spin configuration given by this equation is illustrated in Fig. III-7 where the spin vector precesses at one frequency around the surface of a cone having a half-angle φ'_μ, while the axis of this cone precesses at another frequency around the surface of a second cone having a half-angle φ_μ. We shall revive the spirit of Ptolemy and call such a configuration an epicone spiral. It appears to be the only possible configuration having nonzero Fourier components for just four general $\vec{k}$'s (plus their negatives) and $\vec{k} = 0$.

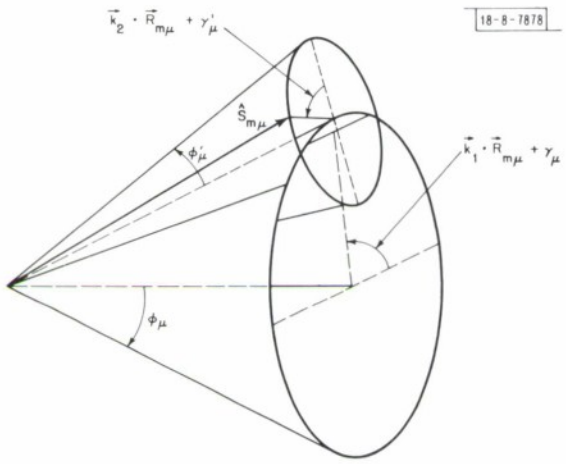

Fig. III-7. An epicone spiral.

An elaborate computer program was written for the IBM 360/67 in order to determine the minimum-energy epicone spiral for any choice of values for the exchange parameters. We find that this epicone has lower energy than the conical spiral when u and $\bar{U}$ are sufficiently large, but it reverts to the cone (φ'_μ becomes zero) approximately along the dashed line shown in Fig. III-6. Since this transition occurs well inside the region where the conical spiral is unstable, the epicone spiral must also be unstable and there must exist yet another configuration with lower energy.

Near the Néel boundary, the minimum-energy epicone has $\vec{k}_1 = (h_o, h_o, 0)$, $\vec{k}_2 = (-2h_o, 0, 0)$, $\vec{k}_1 + \vec{k}_2 = (-h_o, h_o, 0)$, and $\vec{k}_1 - \vec{k}_2 = (3h_o, h_o, 0)$. Kaplan[16] has obtained general expressions for the application of perturbation theory to characterize the destabilizing modes slightly beyond the boundary of the Néel configuration. Preliminary examination of his equations suggests that a Fourier component associated with $\vec{k}_1 + 2\vec{k}_2 = (-3h_o, h_o, 0)$ should also be present. This approach is being pursued.

K. Dwight
N. Menyuk

5. Space-Time Symmetry of Transport Coefficients

Recently, the distinction between symmetry restrictions on equilibrium properties and those on transport properties has been pointed out[17-19] and discussed in some detail.[18-20] The types of symmetry restrictions on the thermogalvanomagnetic (TGM) coefficients occurring for the magnetic field $\underset{\sim}{H} \neq 0$, which were discussed in Ref. 18, have now been examined further.

We find noteworthy, in particular, that it is possible for a Laue group to occur as a group $K^L(\underset{\sim}{H})$ in different categories†: for example, $K^L(\underset{\sim}{H}) = 2'$ has category-case (a)-(iv) when $\underset{\sim}{H}$ is parallel to the 2-fold axis; and $K^L(\underset{\sim}{H}) = 2'$ has category-case (c)-(ii) when $\underset{\sim}{H}$ is perpendicular to the 2-fold axis. Also, category (a) groups $K^L(0)$ have only category (a) subgroups $K^L(\underset{\sim}{H})$, and category (b) groups $K^L(0)$ have only category (b) subgroups $K^L(\underset{\sim}{H})$. However, a category (c) group $K^L(0)$ may, in general, have subgroups $K^L(\underset{\sim}{H})$ of category (a), (b), and/or (c).

The groups $K^L(\underset{\sim}{H})$, which are in category (a) and are subgroups of a group $K^L(0)$ in category (c), were overlooked in the discussion preceding Eq. (3.16) of Ref. 18 and hence were omitted

† The notation and the terms "Laue group," "category," and "case" are defined and discussed in Ref. 18.

from the tables of this reference. The omitted groups $K^{L}(\underset{\sim}{H})$ are 2', 4', and 6' of category-case (a)-(iv), and 2'2'2, 4'22', and 6'22' of category-case (a)-(v). TGM coefficients for 2', 4', and 6' should have been included in Table VIII of Ref. 18; similarly, matrices for 2'2'2, 4'22', and 6'22' should have been included in Table IX. These groups also should have been listed correspondingly in Table III. These omissions are remedied by supplementary tables to be published in the Physical Review.

W. H. Kleiner

B. LASER SCATTERING AND NONLINEAR EFFECTS

1. Velocity and Attenuation of Hypersonic Waves in Liquid Nitrogen

High-resolution thermal Brillouin scattering techniques have been used to measure the velocity and damping of sound in liquid nitrogen in the 3- to 5-GHz range. The measurements were carried out along the saturated vapor line from the triple point to the normal boiling point. Over this range the velocity v in meters/second is well represented by the following linear function of temperature T°K:

$$v = 850.4 + 9.45\,(77.4\text{-}T) \quad . \tag{III-10}$$

This is in agreement with the 1.2-MHz ultrasonic measurements of van Dael, et al.[21] The attenuation has also been measured as a function of frequency and temperature as shown in Fig. III-8.

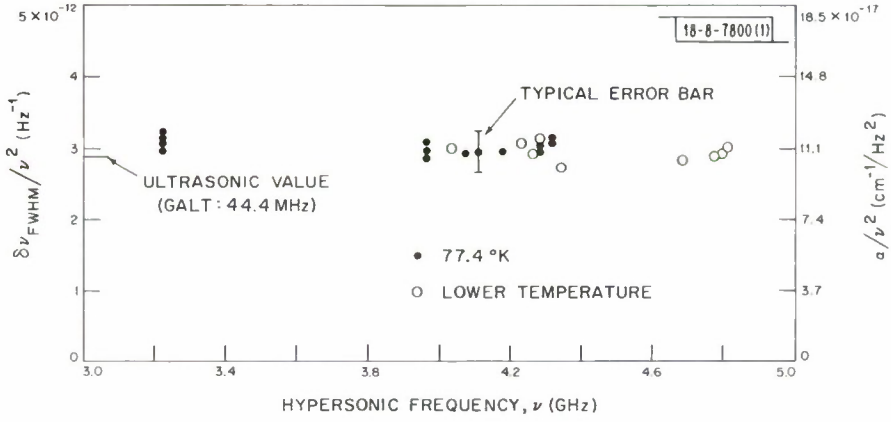

Fig. III-8. Damping of sound in liquid nitrogen.

Within experimental error, the attenuation or linewidth follows the classical ν^2 dependence all the way from the ultrasonic value at 44.4 MHz of Galt[22] to the hypersonic regime. This indicates that acoustic dispersion due to the 2-GHz relaxation frequency of the internal molecular vibration[23] is completely negligible.

A. S. Pine

2. Light Emission from Metals

Light emission using optical excitation has been observed in gold, copper, and gold-copper alloys. This emission involves states near the Fermi level, in contrast to the soft x-ray emission in which the excited holes are in the deep lying bands.

The exciting sources were an argon-ion laser, which could produce in excess of 2 watts CW in either the 4880- or the 5145-Å lines, and a high-pressure Hg arc lamp from which the 3000- to 4000-Å emission bands were used.

Figure III-9 shows the luminescence spectra of gold at 300° and 10°K and copper at 300°K with excitation from the 4880-Å argon laser line. The emission spectra were totally unpolarized and did not vary with polarization of the incident laser beam which is consistent with luminescence from cubic crystals. The spectrum on the long-wavelength side is cut off by the strong absorption near the plasma edge, while the short-wavelength side is limited by the energy available from the pumping source. The emission tail on the high-energy side of the laser occurs from thermal smearing of the electron and hole distributions and, in the case of gold, is seen to disappear at the lower temperature. No correction was made for reabsorption in the present work. Emission observed in copper-gold alloys peaked at wavelengths between that for pure copper and gold. The dependence of the peak emission wavelength on alloy composition was consistent with the absorption thresholds which have been reported recently for Cu-Au alloys.[24]

Details of the excitation and recombination mechanisms are shown in Fig. III-10, where the band structure for a typical noble metal is represented by a simple model which includes an s-p conduction band and two sets of d-bands. The d-bands, indicated by the cross-hatched regions, in fact are made up of a number of closely lying bands in k-space. It seems likely that the emission arises from direct recombination of conduction-band electrons below the Fermi energy with holes in the d-band that have been scattered to momentum states less than the Fermi momentum k_F.

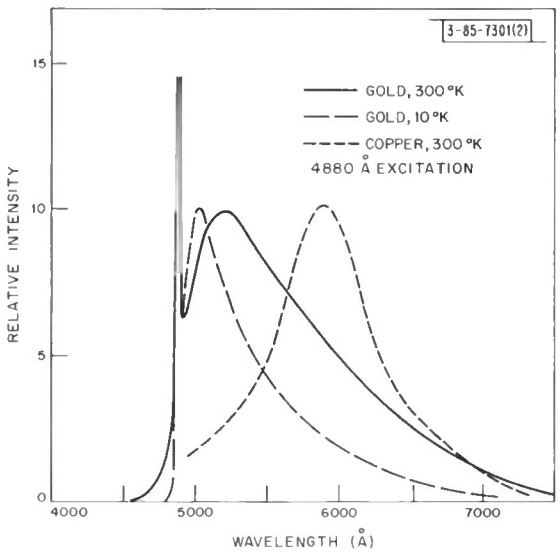

Fig. III-9. Photoluminescence spectra of gold and copper. Exciting light was incident on sample surface at an angle of about 10° from surface, while emitted light was collected normal to surface. Spectra are uncorrected for system response.

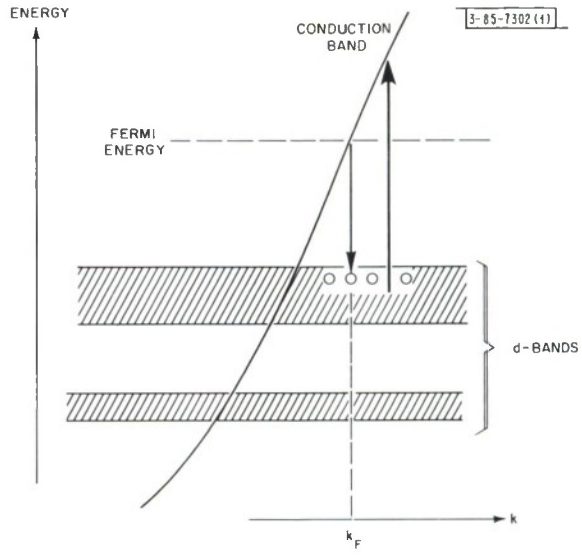

Fig. III-10. Schematic band structure of a noble metal showing excitation and recombination transitions.

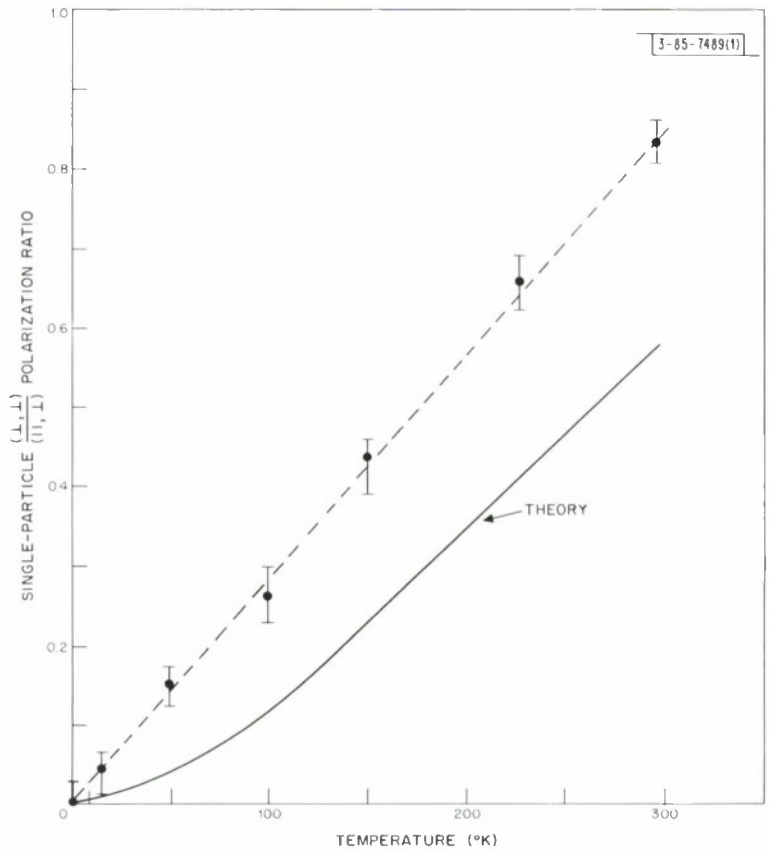

Fig. III-11. Ratia of $(\perp,\perp)$ ta $(\|,\perp)$ scattering crass sectian far single-particle scattering in GaAs (1.4×10^{18} cm^{-3}) as a functian of temperature. The $\|$ and $\perp$ signs refer to palarization of incident laser beam and scottered light relative to plone farmed by incident and scattered prapagatian directions, respectively. Prapagatian was along (100) crystalline axes.

In both metals, the energy for peak emission was consistent with that observed from absorption between the upper d-band and the Fermi energy,[25] namely, 2.0 eV for copper and 2.2 eV for gold. For sufficiently high pump energies, similar transitions between the conduction band and the lower d-band should be observed at around 4 eV. Experiments are in progress, using the 2573-Å output of a doubled argon-ion laser, to observe this transition as well as scattering of light from the single-particle electron excitations.[26] The maximum integrated efficiency of recombination neglecting corrections for reabsorption was estimated to be on the order of 1 part in 10^{10}. A more detailed account of this work is presented elsewhere.[27]

A. Mooradian

3. Anomalous Cross Sections for Light Scattering by Single-Particle Excitations in GaAs

Although most of the anomalously large cross sections observed[26] for light scattering by single-particle excitations in GaAs can be explained[28] in terms of spin-density fluctuations, the large temperature-dependent cross section observed in high-concentration GaAs samples when the incident and scattered polarization vectors are parallel requires a different mechanism. A careful treatment of the effects of resonant enhancement indicates that, despite the very small fluctuations in total charge density, fluctuations in the occupancy of electron states can account for the large cross sections observed for parallel polarization vectors. States of different energy are weighted by different resonant enhancement factors because of the k-dependence of the energy difference between conduction and valence band states. The strong temperature dependence of the polarization properties of the single-particle scattering was found to be in rough agreement with experiment. Figure III-11 shows the theoretical and experimental temperature dependence of the ratio of single-particle scattering with the scattered polarization vectors at 90° to each other. A more detailed account of this work will be published shortly.

A. L. McWhorter
A. Mooradian
D. C. Hamilton

4. Thermal Self-Trapping of CW Laser Beams

Recent experiments[29-31] have produced self-focusing and self-trapping at moderate powers of CW laser beams due to the thermal heating of the medium by the laser beam. The trapping mechanism is the increase produced by the laser in the dielectric constant ($\partial\epsilon/\partial T > 0$).

The steady-state diameter of the self-trapped waveguide was calculated by assuming a dielectric constant of the form

$$\epsilon(T) = \epsilon_o + \frac{\partial\epsilon}{\partial T}\,\Delta T \qquad \text{(III-11)}$$

and simultaneously solving† the heat-flow and wave equations numerically for the field E. Assuming a plane wave $\vec{\mathcal{E}} = \hat{u}E(r)\exp[i(K_o z - \omega t)]$ and neglecting the longitudinal heat flow, longitudinal variation in E, and the imaginary part of K due to the conductivity σ, we find that the dimensionless equations are

† For a mathematically equivalent approach, see F. W. Dabby and H. A. Haus, J. Appl. Phys. 40, 1 (1969).

$$\nabla_{\perp}^2 E = \left(1 - \frac{\omega^2}{\gamma^2 c^2} \frac{\partial \epsilon}{\partial T} \Delta T\right) E \qquad \text{(III-12)}$$

$$\nabla_{\perp}^2 (\Delta T) = - \frac{\alpha c n_o}{8\pi\kappa\gamma^2} |E|^2 \quad . \qquad \text{(III-13)}$$

Here, α = absorption coefficient, κ = thermal conductivity, n_o = index of refraction, and ω = frequency of trapped light. The parameter $\gamma^2 = K^2 - K_o^2$ and is introduced to make the r variable dimensionless in Eqs. (III-12) and (III-13). The boundary conditions are $E = E_o$, $\Delta T = \Delta T_o$, $E' = 0$, and $\Delta T' = 0$ at $r = 0$; $E \to 0$ as $r \to \infty$. For a given value of E_o (ΔT being an adjustable constant), a value of γ is found which gives the trapped mode for E. The values of γ, E_o, and ΔT_o then determine the diameter and power of the beam.

TABLE III-1

THERMAL SELF-TRAPPING HALF-POWER DIAMETERS

Material	$\partial\epsilon/\partial T$ ($^\circ K^{-1}$)	n_a	λ (microns)	a (cm^{-1})	Power (watts)	Diameter at Half Power	
						Thearetical (microns)	Experimental (microns)
Crown glass Nd^+ doping	1.15×10^{-5}†	1.51	0.4880	0.04	0.196	182.0	160 to 200¶
Supercooled water	1.04×10^{-4}	1.336	0.4880	0.05	0.136	51.8	–
Silican	1.27×10^{-3}‡	3.418	10.6	1.33	10.0	95.2#	–
Glass Pb doping	3.5×10^{-5}§	1.75	0.5140	0.08	1.0	27.8	< 50§
Silican	1.27×10^{-3}‡	3.418	1.06	0.05	1.0	162.0	–

† Reference 30.

‡ Determined by A. Mooradian (private communication).

§ Reference 29.

¶ R. Carman (private communication).

Note that in Eqs. (III-12) and (III-13) the imaginary part of K is assumed small compared with the real part. For silicon, this is a poor approximation so that the pawer in the beam is overestimated; hence, the diameter is underestimated.

The calculated half-power diameters for four different materials are listed in Table III-1. These values compare reasonably well with experimental values in the two types of glass.

W. E. Murray, Jr.†
P. L. Kelley‡

† Group 51.

‡ Currently on leave at the Department of Physics, University of California, Berkeley, California.

REFERENCES

1. G. Busch and P. Wachter, Phys. Kanders. Mat. 5, 232 (1966); M.J. Freiser, F. Holtzberg, S. Methfessel, G.D. Pettit, M.W. Shafer, and J.C. Suits, Helv. Phys. Acta 41, 832 (1968).
2. S. Methfessel and D.C. Mattis, Handbuch der Physik (Springer-Verlag, Berlin, 1968), Vol. XVIII, Pt. 1, p. 463.
3. H.S. Jarrett, W.H. Cloud, R.J. Bouchard, S.R. Butler, C.G. Frederick, and J.L. Gillson, Phys. Rev. Letters 21, 617 (1968).
4. V. Johnson, J. Appl. Phys. (to be published) and Ph.D. Thesis, Brown University (1969).
5. K. Adachi, K. Sato, and M. Takeda, J. Phys. Soc. Japan 26, 631 (1969).
6. K. Sato, K. Adachi, T. Okamoto, and E. Tatsumoto, J. Phys. Soc. Japan 26, 639 (1969).
7. M. Hattori, K. Adachi, and H. Nakano, J. Phys. Soc. Japan 26, 642 (1969).
8. N. Menyuk, J.A. Kafalas, K. Dwight, and J.B. Goodenough, J. Appl. Phys. (to be published).
9. D.W. Wood and N.W. Dalton, Phys. Rev. 159, 384 (1967).
10. D.H. Lyons and T.A. Kaplan, Phys. Rev. 120, 1580 (1960).
11. J.S. Smart, Phys. Rev. 86, 968 (1952).
12. D.H. Lyons, T.A. Kaplan, K. Dwight, and N. Menyuk, Phys. Rev. 126, 540 (1962).
13. N. Menyuk, K. Dwight, and A. Wold, J. de Physique 25, 528 (1964).
14. K. Dwight and N. Menyuk, Phys. Rev. 163, 435 (1967), DDC 668194; J. Appl. Phys. 39, 660 (1968), DDC 670771.
15. _____, J. Appl. Phys. 40 (1969), to be published.
16. T.A. Kaplan, Phys. Rev. 119, 1460 (1960).
17. S. Shtrikman and H. Thomas, Solid State Commun. 3, 147 (1965) and erratum in Solid State Commun. 3, No. 9 (1965).
18. W.H. Kleiner, Phys. Rev. 142, 318 (1966), DDC 635328.
19. _____, Phys. Rev. 153, 726 (1967), DDC 653408.
20. Solid State Research Report, Lincoln Laboratory, M.I.T. (1966:2), p. 48, DDC 639064, H-740.
21. W. van Dael, A. van Itterbeek, A. Cops, and J. Thoen, Physica 32, 611 (1966).
22. J.K. Galt, J. Chem. Phys. 16, 505 (1948).
23. W.R.L. Clements and B.P. Stoicheff, Appl. Phys. Letters 12, 246 (1968).
24. P.O. Nilsson, A. Persson, and S. Hagström, Solid State Commun. 6, 297 (1968).
25. D. Beaglehole, Proc. Phys. Soc. (London) 85, 1007 (1965), and 87, 461 (1966).
26. A. Mooradian, Phys. Rev. Letters 20, 1102 (1968), DDC 671287.
27. _____, Phys. Rev. Letters 22, 185 (1969).
28. D.C. Hamilton and A.L. McWhorter, Proceedings of the International Conference on Light Scattering Spectra of Solids (Springer-Verlag), to be published.
29. F.W. Dabby and J.R. Whinnery, Appl. Phys. Letters 13, 8 (1968).
30. R.L. Carman, A. Mooradian, P.L. Kelley, and A. Tufts, Appl. Phys. Letters 14, 4 (1969).
31. A.G. Litvak, JETP Lett. 4, 230 (1966).

DOCUMENT CONTROL DATA – R&D

(Security classification of title, body of abstract and indexing annotation must be entered when the overall report is classified)

1. ORIGINATING ACTIVITY *(Corporate author)* Lincoln Laboratory, M.I.T.	2a. REPORT SECURITY CLASSIFICATION Unclassified 2b. GROUP None

3. REPORT TITLE

Solid State Research

4. DESCRIPTIVE NOTES *(Type of report and inclusive dates)*

Quarterly Technical Summary – 1 February through 30 April 1969

5. AUTHOR(S) *(Last name, first name, initial)*

Tannenwald, Peter E.

6. REPORT DATE	7a. TOTAL NO. OF PAGES	7b. NO. OF REFS
15 May 1969	60	76

8a. CONTRACT OR GRANT NO. AF 19(628)-5167 b. PROJECT NO. 649L c. d.	9a. ORIGINATOR'S REPORT NUMBER(S) Solid State Research (1969:2) 9b. OTHER REPORT NO(S) *(Any other numbers that may be assigned this report)* ESD-TR-69-110

10. AVAILABILITY/LIMITATION NOTICES

This document has been approved for public release and sale; its distribution is unlimited.

11. SUPPLEMENTARY NOTES	12. SPONSORING MILITARY ACTIVITY
None	Air Force Systems Command, USAF

13. ABSTRACT

This report covers in detail the solid state research work at Lincoln Laboratory for the period 1 February through 30 April 1969. The topics covered are Solid State Device Research, Materials Research, and Physics of Solids. The work formerly reported by the Optics and Infrared Group will henceforth appear in a separate report entitled "Optics Research" to be issued by the Optics Division.

14. KEY WORDS

solid state devices
materials research
magnetism
laser scattering
magnetospectroscopy
infrared
crystal growth
laser research
ion implantation
Brillouin scattering